This is to certify that the

thesis entitled

THE POTENTIAL ENERGY SURFACE AND PARTIAL MOLAR HEAT CAPACITY OF INTERSTITIAL HYDROGEN IN THE YTTRIUM DIHYDRIDE SYSTEM

presented by

Keith Michael Glassford

has been accepted towards fulfillment of the requirements for

MS degree in Chem Engr

Robert E. Buxbaum

Major professor

Date May 5, 1992

THE POTENTIAL ENERGY SURFACE AND PARTIAL MOLAR HEAT CAPACITY OF INTERSTITIAL HYDROGEN IN THE YTTRIUM DIHYDRIDE SYSTEM

By

Keith Michael Glassford

A THESIS

Submitted to

Michigan State University

in partial fulfillment of the requirements

for the degree of

MASTERS OF SCIENCE

Department of Chemical Engineering

1992

ABSTRACT

THE POTENTIAL ENERGY SURFACE AND PARTIAL MOLAR HEAT CAPACITY OF INTERSTITIAL HYDROGEN IN THE YTTRIUM DIHYDRIDE SYSTEM

By

Keith Michael Glassford

The anomalous occupation of octahedral sites by hydrogen in the yttrium dihydride system is examined by modeling the interstitial partial molar heat capacity and hydrogen potential energy surface. The total heat capacity is separated into optical, acoustical, and configurational contributions. Theoretically predicted heat capacities are in good agreement with experiment at high temperatures, while the low temperature values are underestimated by approximately 1 cal/mol deg. This discrepancy is attributed to hydrogen-hydrogen interactions, configurational effects and entropic terms arising from the metal lattice.

The hydrogen potential energy surface has been calculated along high symmetry directions of the metal sublattice using an effective medium formalism. Hydrogen-hydrogen interactions hybridization effects are neglected. The resulting energy surfaces were found to be strongly dependent upon the configuration of the free atom. Diffusion paths and embedding energies are in qualitative agreement with experiment.

To my parents

Bettie Jane and Douglas Michael Glassford

for their love, support, and encouragement

which made it all possible

ACKNOWLEDGMENTS

I would like to thank my parents, Bettie and Doug Glassford, and my wonderful sisters: Diane, Roxane, and Dárcy for their constant source of love and encouragement. I owe much of my success to them as they have helped in shaping who I am.

I thank my thesis advisor, Prof. Robert E. Buxbaum, who has been an inspiration to me since my earliest days of science. I owe much of my love of science to him as he shown me the blue prints of how to be a great scientist. His constant encouragement and guidance will never be forgotten.

A special thanks to my dear friends Kevin Jacques and Bharath Rangarajan who stood there with me in through the worst and best of times. I thank them for always having a shoulder to lean on and listening ear.

TABLE OF CONTENTS

LIST OF TABLES

LIST OF FIGURES

CHAPTER 1

MODELING HYDROGEN IN METALS

1.1 General overview

The technological importance of the hydrogen in metals and a practical need for fundamental understanding of hydrogen embrittlement, hydrogen storage, hydrogen pumping and separation, and fusion technology have prompted a wealth of experimental and theoretical work [1]. The ability to predict accurate thermodynamic and kinetic information for metal hydrides requires a detailed knowledge of the hydrogen-metal and hydrogen-hydrogen interactions. The goal of the present research is to examine and develop engineering application of methodologies for H in metals, and to use these methodologies to predict the potential energy surface for hydrogen in yttrium dihydride.

Theoretical studies of metal hydride systems, denoted MH_x, have concentrated on low hydrogen to metal ratios: $x \ll 1$. Here, hydrogen-hydrogen interactions are weak compared to metal-metal and metal-hydrogen interactions and are usually ignored. However, in many engineering systems, $x \gg 1$ and hydrogen-hydrogen interactions are important if only to to explain the various hydride phases. Hydrogen-hydrogen interactions may be classified as either short range (direct) or long range (elastic). Short range interactions are transferred directly through the H-H potential; whereas, long range elastic interactions are transferred through the displacement field of the surrounding metal atoms. For example, in PdH_x, the H-H interaction has a short

range repulsive component and a long range, lattice mediated, attraction [2]. The lattice mediated interaction allows H-H pairs to share the elastic strain energy of the expanding metal lattice, permitting hydrogen absorption; whereas, the repulsive interactions inhibit tetrahedral site occupation. This occupation is why Pd absorbs only one H per metal atom situated in the O site [2].

A hydrogen potential energy surface describes the energy for hydrogen motion through a metal lattice including both short range and elastic interactions. In describing this energy surface one must consider not only the type and chemical nature of the host metal but also the hydrogen concentration, temperature, and pressure of the system. An important simplification arises when one considers the small mass of the hydrogen atom compared to a typical transition metal atom. The resulting mass difference leads to the notion of two different time scales, i.e., one for the hydrogen motion and one for the metal atom vibrations. This allows one to treat the problem as though hydrogen is diffusing through a static metal lattice of *infinite* mass. These two time scales become apparent when one considers the vast difference of the diffusion coefficient of hydrogen in a transition metal hydride compared to the self diffusion of the metal atoms, typically orders of magnitude.

In order to determine the potential energy surface for the diffusing hydrogen atom, one usually invokes the Born-Oppenheimer approximation; whereby, Schrödingers wave equation is solved for the the electronic energy at various fixed nuclear configurations along the diffusion path. Typically, embedding a hydrogen atom into the bulk metal causes an outward relaxation of the surrounding metal atoms; the extent of lattice relaxations depends upon the balance between the loss of energy due to lattice distortions and gain in the H impurity energy [7]. This so called self-trapped state, has been used to describe phonon assisted tunnelling between interstitial sites, as in the small polaron theory of Flynn and Stoneham [4]. The self-trapped state may be envisioned as the H atom "digging" a deeper potential well for itself; thereby,

minimizing its energy at the expense of lattice distortions.

The theoretical description of defect and impurity induced lattice distortions, within the harmonic approximation, was initially developed by Kanzaki [5], and has been extended to to include the Green function formalism [6,7,8]. The atomic displacements of the metal atoms, due to the presence of the hydrogen atom, may be calculated from a knowledge of the perfect lattice Green function and the Kanzaki force exerted by the H atom on the surrounding metal atoms [9]. The relaxation energy, in turn, is calculated from the atom displacements and the hydrogen induced forces; which in principle, should be calculated quantum mechanically from the H potential and wave function [9]. The problem must therefore be solved self consistently to obtain the surrounding metal atom relaxations. The H binding energy is comprised of electronic and vibrational contributions, i.e., a well depth plus a zero point energy. The hydrogen local mode frequencies may be determined by solving Schrödinger's equation for the impurity wave function [9,10,12,13] using the relaxation method of Kimball and Shortley [14]. However, for transition metals, the quantum effects are usually only a small part of the total energy [3], as well as the relaxation energy for close-packed metals [7]. Thus, a detailed knowledge of the hydrogen potential energy surface is needed to determine the dynamics of hydrogen in transition metals, whether or not local lattice relaxations are included.

1.2 Hydrogen Potential Energy surface

Due to the complexity of the many-body potential, most solid state potential energy surfaces are modeled by deconvoluting the interactions into pairwise additive potentials between atoms [16]-[18] such as Morse, Lenord-Jones and Born-Mayer potentials. The pair potential parameters are then fit to various structural and energetic properties of the bulk crystal, i.e., experimental lattice constant and cohesive energy. Ideally, the chosen potential should be able to model all the physics of the system.

Unfortunately, this is usually not the case, whereas fitting different data may lead to vastly different property predictions. One must therefore be careful to chose data which is sensitive to that being modeled. The main advantage of the pair potential formalism is the ease at which molecular dynamic simulations may be performed. However, as stated above, the validity of the potential parameters become questionable far from equilibrium. One must check whether the answers obtained from the model are physical and represent a viable prediction or whether they are an artifact of the fit. For the dynamics of hydrogen in metals, at low hydrogen concentrations, the modeling is somewhat easier. Due to the high diffusivity of H, relative to the self diffusion of the metal atoms, the potential often can be parameterized by experimental data which directly probes the H-M interactions [19,9,20,21,22,10], e.g., heat of solution, activation energy for hydrogen diffusion and local mode vibrational frequencies. If the hydrogen motion does not strongly distort the metal sublattice one may thus eliminate the need for modeling the M-M interactions. Use of this type of potential is limited as the experimental data used for fitting the H-M potential are often precisely those which are to be predicted by the model.

Inherently, neglect of the M-M potential assumes that, as the H atom diffuses through the bulk hydride, its influence on the surrounding metal atoms being negligible. As discussed in the previous section, distortion of the surrounding metal atoms may be important in describing the hydrogen dynamics. One might wish, then, to model M-M interactions by pair potentials obtained from experimental data on the pure metal. However, pair potentials have serious shortcomings in modeling elastic properties. Specifically, pair potentials lead the Cauchy discrepancy [12], i.e., $C_{12} = C_{44}$ which is rarely observed in transition metals. Here C_{ij} are the elastic constants for the crystal in Voigt notation [9]. The inadequacy of local pairwise M-M interactions demonstrates the importance of three body and volume dependent terms in the many-body expansion.

Daw and Baskes [23] developed a semi-empirical, volume dependent formalism based on density functional theory. The parameters of their model are fit to experimental data probing the M-M and H-M interactions as above, and the volume dependence is calculated via the free atom electron density. This method does not predict the Cauchy discrepancy and is well suited for describing surrounding metal atom relaxations. However, as before, the experimental data needed usually include what one hopes to predict. Moreover, experimental data directly probing the M-H interactions is often lacking. To alleviate the need for experimental data, Jacobsen *et al.* [11] have, extended the method by developing an effective medium approach, using the variational principle of density functional theory. In their method, the parameters are calculated within the local-density approximation, in a self consistent fashion, yielding potentials which are in principle, valid away from the equilibrium structure of the crystal. For a review of interatomic interactions based on the effective medium approach, the reader is referred to Manninen [26].

Fundamentally, the potential energy surface of hydrogen in a transition metal host may be described by its site dependent embedding energy (or binding energy). The embedding energy of hydrogen in a metal host, is defined as the difference between the total energies of the combined hydrogen-metal system and the energies of the separated hydrogen and host metal:

$$\Delta E = E[M + H] - E[M] - \frac{1}{2}E[H_2]. \tag{1}$$

Here, $E[M + H]$ is the energy of the host metal with the embedded hydrogen atom, $\frac{1}{2}E[H_2]$ and $E[M]$ are the energies of the separated hydrogen atom and host metal respectively. Formally, $E[M + H]$ includes lattice relaxations around the hydrogen atom and $E[M]$ is evaluated at the structure of the metal lattice before embedding. Equation 1 gives basically the electronic contribution to the energy of a hydrogen atom; as discussed in Section 1.1, the hydrogen vibrational energy must be added to

obtain the total site energy. Approaches used to solve for the hydrogen embedding energy range from empirical models to fully self-consistent *ab initio* calculations.

One way of simplifying Eq. 1 involves separating out the relaxation energy of the metal atoms:

$$E[M+H] = E_{st}[M+H] + \Delta E_R \tag{2}$$

where $E_{st}[M+H]$ is the static energy of the perfect lattice with embedded hydrogen, and ΔE_R is the change in energy due to relaxation of the surrounding metal atoms, as discussed in Section 1.1. This allows much more simple models for predicting the lattice relaxation energy, and alleviates the need for a full phase space optimization of the atomic coordinates.

In the case of large x, Eq. 1 must be further modified to account for the presence of neighboring hydrogen atoms, the high H concentration analog of Eq. 1 being:

$$\Delta E = E[M+H_{n+1}] - E[M+H_n] - \frac{1}{2}E[H_2]. \tag{3}$$

Equation 3 is more difficult to solve than Eq. 1, in that the H-H interactions are included but their form or strength are not known *a priori* and depend upon the metal host.

1.3 Self Consistent Calculations

In stoichiometric, ordered hydrides, self-consistent total energy calculations have been performed using a linear combinations of muffin tin orbitals (LMTO), linear combination of atom orbitals (LCAO), or Korringa-Kohn-Rostoker (KKR) [38] have been performed as well as the Green function method within the LMTO atomic sphere approximation (ASA) for hydrogen impurity states [39]. These methods are valuable for understanding effects peculiar to ordered systems. However, when one hydrogen

moves off site, as in diffusive motion, the loss of translational periodicity of the lattice greatly increases the computational complexity and cost of these methods. In order to deal with the loss of translational periodicity two methods have evolved to describe the diffusion of impurity atoms: (*i*) the cluster approach and (*ii*) the supercell method.

In the cluster approach, the infinite crystal is modeled as a finite cluster of atoms in vacuum. The total energies of the molecular clusters with and without the hydrogen atom are calculated quantum mechanically and the embedding energy is calculated from Eq. 1 or 3. Self consistent LCAO-MO calculations [27] have been performed on Li_nH using an unrestricted Hartree-Fock method. Structural properties where found to converge at relatively small cluster sizes where only three atoms were needed to correctly describe the ordering of the sc, fcc and bcc stability! However, the hydrogen embedding energy varied strongly with cluster size and geometry [27]. The problem of convergence, invariably inhibits the method due to the long range nature of the interactions; however, much of the basic physics is still present and may provide an adequate approach in some systems were the range of interactions is not as large.

The supercell technique [28] restores the translational periodicity of the lattice by placing the defect in a large unit cell. One then usually solves Schrödingers wave equation within the framework of density functional theory [6]. The major simplification in this methodology is that the cohesion in solids largely results from valence electrons. One thus replaces the potential seen by the valence electrons by a pseudopotential [37] which explicitly replaces the core electrons. It is assumed that the potential which the valence electrons experiences is the same whether the core is present in atomic, molecular or crystalline form. This leads to a drastic simplification of the problem due to the decrease in the number of electrons. For a single defect one constructs a supercell which is large enough that the interactions between defects in different cells is minimized. In the case of hydrogen this is easily achieved as the

valence electrons effectively screen the hydrogen potential. Calculations have been performed for hydrogen trapping by substitutional impurities in semiconductors [30] hydrogen adsorption on Ru(0001) [31], Pd(001) [32], Be(0001) [33], and hydrogen diffusion in Nb [34], Pd [35] and Si [36]. These *ab initio* or first-principles results have compared well with experiment and have helped in a theoretical understanding of hydrogen on the surface and in the bulk phase of hydrogen metal systems. The computational complexity and cost of this method remains high; it does however, provide a means for benchmark calculations for developing more empirical, less costly methods for calculations of hydrogen in transition metals.

LIST OF REFERENCES

[1] *Hydrogen in Metals I*, edited by G. Alefeld and J. Völkl, Topics in Applied Physics, Vol. **28**, (Springer Verlag, Berlin, 1978); *Hydrogen in Metals II*, edited by G. Alefeld and J. Völkl, Topics in Applied Physics, Vol **29**, (Springer Verlag, Berlin, 1978)

[2] O. B. Christensen, P. D. Ditlevsen, K. W. Jacobsen, P. Stoltze, O. H. Nielsen, and J. K. N ørskov, Phys. Rev. B **40**, 1993 (1989).

[3] P. Nordlander, J. K. Nörskov, and F. Besenbacher, J. Phys. F **16**, 1161 (1986).

[4] C. P. Flynn and A. M. Stoneham, Phys. Rev. B **1**, 3966 (1970).

[5] H. Kanzaki, J. Phys. Chem. Solids **2**, 24 (1973).

[6] V. K. Tewary, Adv. Phys. **22**, 757 (1973).

[7] A. A. Maradudin, E. W. Montroll, G. H. Weiss, and I. P. Ipatoua, *Theory of Lattice Dynamics in the Harmonic Approximation*, edited by H. Ehrenreich, F. Seitz, and D. Turnbull, Solid State Phys. Suppl, Vol. **3**, 2nd Ed. (Academic Press, New York, 1971).

[8] I. R. MacGillivray and C. A. Sholl, J. Phys. F **13**, 23 (1983).

[9] H. Sugimoto and Y. Fukai, Phys. Rev. B **22**, 670 (1980).

[10] H. Sugimoto and Y. Fukai, J. Phys. Soc. Jpn. **50**, 3709 (1981).

[11] N. W. Ashcroft and N. D. Mermin, *Solid State Physics* (Saunders College, Philadelphia, 1976).

[12] M. Born and K. Haung,*Dynamical Theory of Crystal Lattices*, (University Press, Oxford, 1954).

[13] M. Manninen, Phys. Rev. B **34**, 6886 (1986).

[14] G. E. Kimball and G. H. Shortley, Phys. Rev. **45**, 815 (1934).

[15] M. J. Puska and R. M. Nieminen, Phys. Rev. B **29**, 5382 (1984).

[16] R. A. Johnson, J. Phys. F **3**, 295 (1973).

[17] A. J. Pertsin and A. I. Kitaigorodsky, *The Atom-Atom Potential Method*, Springer Series in Chem. Phys., Vol. **43** (Springer Verlag, Berlin, 1987).

[18] R. A. Johnson and W. D. Wilson, in *Interatomic Potentials and Simulation of Lattice Defects*, edited by P. C. Gehlen, J. R. Beeler, and R. I. Jaffe, (Plenum, New York, 1971) pp. 301.

[19] D. R. Olander, J. Phys. Chem. Solids**32**, 2499 (1971).

[20] G. Wahnström, J. Chem. Phys. **89**, 6996 (1988).

[21] S. M. Valone, A. F. Voter, and J. D. Doll, Surf. Sci. **155**, 687 (1985).

[22] S. Ikeda and N. Watanabe, J. Phys. Soc. Jpn. **56**, 565 (1987).

[23] M. S. Daw and M. I. Baskes, Phys. Rev. Lett. **50**, 1285 (1983); M. S. Daw and M. I. Baskes, Phys. Rev. Lett. **29**, 6443 (1984).

[24] S. M. Foiles, M. I. Baskes, and M. S. Daw, Phys. Rev. B **33**, 7983 (1986).

[25] K. W. Jacobsen, J. K. Nörskov, and M. J. Puska, Phys. Rev. B **35**,7923 (1987).

[26] M. Manninen, Phys. Rev. B **34**, 8486 (1986).

[27] B. K. Rao and P. Jena, J. Phys. F **16**, 461 (1986).

[28] M. L. Cohen, M. Schlüter, J. R. Chelikowsky, and S. G. Louie, Phys. Rev. B **12**, 5575 (1975); M. Schülter, J. R. Chelikowsky, S. G. Louie, and M. L. Cohen, Phys. Rev. B **12**, 4200 (1975).

[29] P. Hoenberg and W. Kohn, Phys. Rev. **136**, B864 (1964); W. Kohn and L. J. Sham, Phys. Rev **140**, A1134 (1965).

[30] P. J. H. Denteneer, C. G. Van de Walle, and S. T. Pantelides, Phys. Rev. Lett. **62**, 1884 (1989).

[31] M. Y. Chou and J. R. Chelikowsky, Phys. Rev. Lett.**59**, 1737 (1987).

[32] D. Tománek, S. G. Louie, and Che-Ting Chan, Phys. Rev. Lett. **57**, 2594 (1986).

[33] R. Yu and P. K. Lam, Phys. Rev. B **39**, 5035 (1989).

[34] K. M. Ho, H. J. Tao, and X. Y. Zhu, Phys. Rev. Lett.**53**, 1586 (1984).

[35] Z. Sun and D. Tománek, Phys. Rev. Lett. **63**, 59 (1989).

[36] C. G. Van de Walk, Y. B. Yam, and S. T. Pantelides, Phys. Rev. Lett. **60**, 2761 (1988)

[37] M. Schlüter and C. Chiang, Phys. Rev. Lett. **43**, 1494 (1979).

[38] D. K. Misemer and B. N. Harmon, Phys. Rev. B **26**, 5636 (1982).

[39] O. Gunnarsson, O. Jepsen, and O. K. Andersen, Phys. Rev. B **27**, 7144 (1983).

CHAPTER 2

YH_2 SYSTEM: EXPERIMENTAL OVERVIEW

2.1 Introduction

The technological importance of hydrogen in metals has generated a wealth of experimental information for a number of systems. The yttrium hydride system has received a great deal of attention in the last decade not only due to its ability to absorbed large amounts of hydrogen but also to its inherent ability to absorb hydrogen into octahedral sites before complete tetrahedral occupancy has been achieved. The following chapter reviews the current experimental information relevant to the diffusion mechanism as well as the anomalous octahedral site occupancy. In Section 2.2 the yttrium hydride system is presented

2.2 The YH_x Phase Diagram

Yttrium is a transition metal of the group III-A and occurs in the hexagonal close-packed (hcp) crystal structure. Upon adsorbing hydrogen, the yttrium lattice undergoes phase changes to accommodate the hydrogen atoms. The phases of YH_x, as a function of temperature and hydrogen to metal ratios $x \leq 3$, are shown in Figure 1. In the hcp structure, yttrium metal absorbs small amounts of hydrogen to form the α-YH_x solid phase solution. The hcp lattice is shown in Figure 2 where open circles represent the metal atoms and the the solid circles are possible tetrahedral (T) and Octahedral (O) sites available for hydrogen occupancy. There are two T and

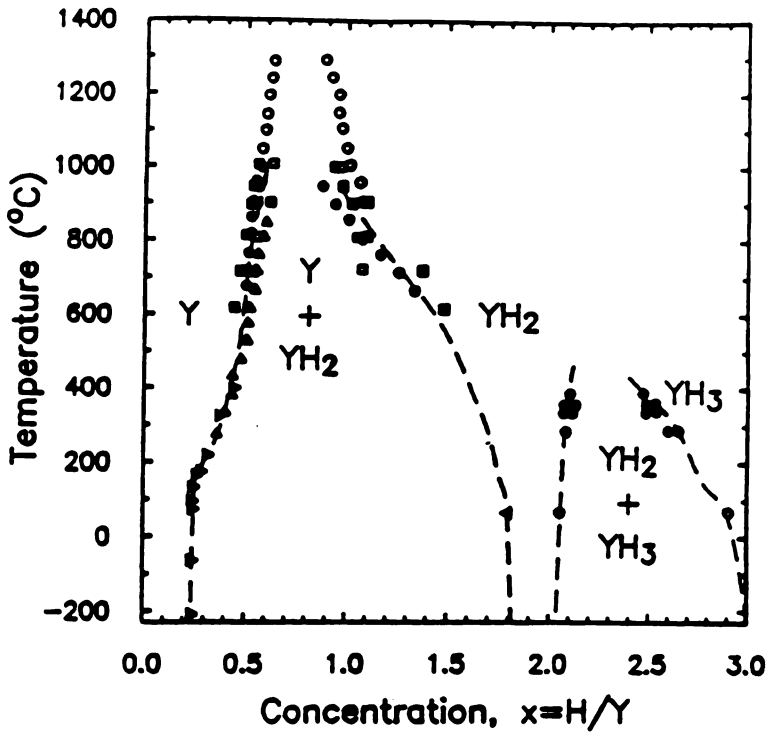

Figure 1: YH_2 Phase diagram (Markert, 1987)

one O site per metal atom in the hcp structure. While these sites have the highest "volume" and symmetry, other sites exist due to Jahn-Teller symmetry breaking [1], lattice distortions, or hydrogen-hydrogen interactions. In the α-YH_x solid solution, hydrogen atoms almost exclusively occupy the low energy T sites [2]. The α-phase boundary remains relatively constant at $x = 0.24$ until temperatures exceed 400 K [3]. This shows that the hydrogen atoms are interacting, as otherwise the phase boundary would approach $x = 0$ at low temperatures [3]. Initially, it was proposed that hydrogen atom pairing at nearest neighbor T sites [4] was responsible for this behavior; but proton NMR studies [3] on $YH_{0.2}$ found no evidence of the doublet peak characteristic of the proposed pairing. Resistivity studies [5], diffuse neutron scattering [6], and inelastic neutron scattering experiments [7] have conclusively shown

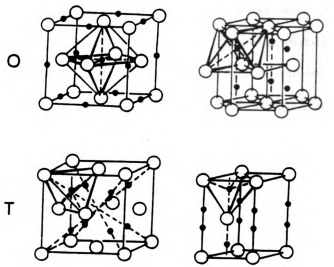

Figure 2: Crystal structure of the yttrium metal sublattice in the hcp and fcc crystal structures showing possible tetrahedral and octahedral hydrogen sites (Fukai and Sugimoto, 1985)

that pairing does occur, but along the c-axis between next-nearest neighbor hydrogen atoms rather than the nearest neighbors. At higher temperatures the H-H pairs "decompose" into "free" atoms in solution leading to "normal" behavior of the phase boundary [8].

At higher hydrogen concentrations, the yttrium lattice rearranges to a face centered cubic (fcc) dihydride, $YH_{2\pm\delta}$ structure which the present work concentrates upon. Figure 1 shows that this dihydride is stable over a large range of non-stoichiometric compositions. Even at low temperatures, this concentration range is approximately $1.8 \leq x \leq 2.1$ [9]. As with the hcp lattice, the fcc lattice has two T and one O sites per metal atom, with H largely occupying T sites [17]. These interstitial sites are shown in Figure 2. Increasing the hydrogen concentration further, causes rearrangement of the yttrium lattice back to an hcp structure where both O and T interstitial sites are occupied significantly. This is the nonstoichiometric trihydride in Figure 2.2.

2.3 Hydrogen Site Occupancy and motion in YH_x

A great deal of work has been performed to understand the variance in site occupancy for the transition metal hydrides This is important to understand the thermodynamical and transport properties and to provide a deeper understanding of hydride formation and the various trends for different transition and simple metal hydrides. An important aspect of this involves the strong hydrogen-metal d-band interactions [11], or hybridization effects commonly seen is sp^3 type semiconductors such as silicon. As one moves from right to left of the periodic table, these hybridization effects become more pronounced due to the larger number of unoccupied states which the hydrogen s states can interact. The degree of this interaction largely depends upon the location of these empty states relative to the Fermi energy and can be probed by techniques which probe the electronic structure of the material, *eg.*, photoemission, absorptivity, and thermoreflectance experiments.

The optical properties of YH_x have been studied by Weaver *et al* [12] for $1.73 \leq x \leq 1.98$ using optical absorptivity and thermoreflectance techniques. The optical properties where found to be strongly dependent upon the hydrogen concentration. As $x \rightarrow 2$, a new interband absorption was observed for photon energies near the Fermi level. This increase in absorption is due to hydrogen-derived states near the Fermi energy and could not be describe by interband transitions for YH_2 in the CaF_2 structure [13,11]. Rather it was assumed that O site occupancy was responsible for these new interband transitions [12]. The optical absorptivity of $YD_{1.88}$ show this same low energy structure also, presumably due to O site occupancy [12]. Temperature effects in the optical absorptivies and conductivity spectra also result in an attenuation of a low energy peak, presumably due to the proposed O site occupancy [12]. Photoelectron energy distributions from synchrotron radiation experiments [14] showed further evidence for O site occupation through an increase in emission from the conduction band as $x : 1.73 \rightarrow 1.98$ [14]. These observations of O site occupancy are supported by supercell calculations [15] for non-stoichiometric Y_4H_9, Y_4H_{11}, and Y_4H_{12} corresponding to an O site occupancy of 1/4, 3/4, and 1 respectively. Generally the addition of an H atom to an O site lowered an unoccupied band near the Fermi energy for each additional atom [15] added to an O site. These bands being responsible for enhanced optical absorptivities [12].

Considering that the fcc YH_2 structure has two low energy T sites per metal atom, one would expect that H atoms in the deficient dihydride would occupy the lower energy T sites before spilling over to the higher energy O sites at $x \geq 2$. However, various experiments including electron spin resonance [16,17], proton nuclear magnetic resonance [3,8,18,19], neutron diffraction [15,17,20], inelastic neutron scattering [15,17] and μ spin rotation [11] have confirmed and quantified this premature filling of O sites.

Nuclear magnetic resonance (NMR) provides a valuable tool for studying H mobility in hydrides, and to some extent the site occupancy. The technique is applicable to any isotope having a magnetic moment [2]. Two experimental techniques used in NMR diffusion studies are: *i*) spin lattice relaxation measurements and *ii*) the pulsed-field-gradient method, the later being a direct measure of the intrinsic diffusion [18]. The stability of the dihydride phase allows NMR experiments to probe hydrogen mobility over a wide range of composition and temperatures. However, the accuracy of NMR determinations of site occupancy is questionable, because of the temperature insensitivity and inaccuracies in the proton resonance second moment, M_2, lead to errors in site occupancy determinations of approximately ±20% [8,17,18].

Using NMR pulsed-field-gradient techniques in the temperature range 140 - 760 K, Anderson *et al.* [18] observed three temperature ranges exhibiting vastly different activation energies for proton motion in YH_x for x = 1.63, 1.92 and 1.98. The experimental jump frequencies and activation energies in these three temperature regions are given Table 1; the jump frequency being given as $\nu_j = \nu_0 \exp(-E_{act}/k_B T)$ where E_{act} is the activation energy for H diffusion, k_B is Boltzmann's constant and T is the absolute temperature. The inverse of the jump frequency also gives the mean residence time, $\tau_D = \nu_j^{-1}$, for the proton at the particular site. Further, the two phase $YH_{1.63}$ sample gave H diffusivities three orders of magnitude lower than in the dihydride phase; activation energies being approximately two times greater than in the later [18]. Using proton spin lattice relaxation techniques, Markert [9] found similar variations in activation energies for hydrogen diffusion in the dihydride phase. Thus the motion of hydrogen in the dihydride phase does not follow the usual linear Arrhenius behavior; the later study by Markert showed that a distribution of activation energies rather than a single energy resulted in a better agreement with experiment [9].

To explain this non-Arrhenius diffusion behavior, Andersen [18] has proposed that

Table 1: Experimental jump frequencies for hydrogen in YH_x, taken from [18]

$YH_{1.63}$			
Region	T_{trans}(K)	$\nu_0(s^{-1})$	E_{act}
I	465	$4.5 \cdot 10^{8}$	0.457
II	600	$1.45 \cdot 10^{13}$	0.877
III	—	$1.066 \cdot 10^{15}$	1.1

$YH_{1.92}$			
Region	T_{trans}(K)	$\nu_0(s^{-1})$	E_{act}
I	280	$2.35 \cdot 10^{7}$	0.208
II	370	$1.80 \cdot 10^{9}$	0.308
III	—	$1.58 \cdot 10^{11}$	0.438

$YH_{1.98}$			
Region	T_{trans}(K)	$\nu_0(s^{-1})$	E_{act}
I	270	$6.96 \cdot 10^{7}$	0.218
II	330	$1.052 \cdot 10^{10}$	0.336
III	—	$1.58 \cdot 10^{11}$	0.417

the motion of hydrogen on both the T and O YH_2 sublattice must be considered. Low temperature H diffusion was attributed to motion between O sites whereupon increasing temperatures exchange occurs between both O and T sites and at high temperatures, diffusion occurs between all diffusion paths [18]. This is consistent with premature octahedral site occupation eluded to in the beginning of this section. Recent INS experiments by Goldstone *et al.* [17], on YH_2 found the octahedral occupation, x_0, to be approximately constant ($x_0 \sim 8\%$) at temperatures below 200 K, decreasing with increasing temperature; presumably due to entropic contributions from the Y lattice. Thus at low temperatures, the sizable fraction of occupied O sites, approximately 8%, provides a relatively small diffusion barrier for the T-O path. As temperature is increased the O site occupation decreases dramatically and H diffuses *via* the larger barrier T-T path.

LIST OF REFERENCES

[1] A. Klamt, J. Phys. F **17**, 47 (1987).

[2] D. Katamian, C. Stassis, and B. J. Beaudry, Phys. Rev. B **23**, 624 (1981).

[3] L. Lichty, R. J. Schoenberger, D. R. Torgeson, and R. G. Barnes, J. Less-Common Metals **129**, 31 (1987).

[4] C. V. Owens and T. E. Scott, J. Less-Common Metals **90**, 275 (1983).

[5] P. Vajda, J. N. Daou, A. Lucasson, and J. P. Burger, J. Phys. F **17**, 1029 (1987).

[6] M. W. McKergow, D. K. Ross, J. E. Bonnet, I. S. Anderson, and O. Schaerpf, J. Phys. C **20**, 1909 (1987).

[7] I. S. Anderson, N. F. Berk, J. J. Rush, and T. J. Udovic, Phys. Rev. B **37**, 4358 (1988).

[8] D. L. Anderson, R. G. Barnes, D. T. Peterson, and D. R. Torgeson, Phys. Rev. B **21**, 2625 (1980).

[9] J. T. Markert, Ph.D. Thesis, Cornell University (1987).

[10] J. A. Goldstone, J. Eckert, P. M. Richards, and E. L. Venturini, Solid State Comm.**49**, 475 (1984).

[11] A. C. Switendic, Int. J. Quantum Chem. **5**, 459 (1971).

[12] J. H. Weaver, R. Rosei, and D. T. Peterson, Phys. Rev. B **19**, 1855 (1979).

[13] D. J. Peterman, B. N. Harmon, J. Marchiando, and J. H. Weaver, Phys. Rev. B **19**, 4867 (1979).

[14] J. H. Weaver and D. T. Peterson, J. Less-Common Metals **74**, 207 (1980).

[15] A. C. Switendic, J. Less-Common Metals **74**, 74 (1980).

[16] E. L. Venturini and P. M. Richards, Phys. Lett. **76**A 344 (1980).

[17] E. L. Venturini, J. Less-Common Metals **74**,45 (1980).

[18] D. L. Anderson, R. G. Barnes, T. Y. Hwang, D. T. Peterson, and D. R. Torgeson, J. Less-Common Metals **73**, 243 (1980).

[19] R. G. Barnes, F. Borsa, M. Jeroshch-Herold, J. -W. Han, M. Belhoul, and E. F. W. Seymour, J. Less-Common Metals **129**, 279 (1987).

[20] D. Khatamian, W. A. Kamitakahara, R. G. Barnes, and D. T. Peterson, Phys. Rev. B **21**, 2622 (1980).

[21] J. A. Goldstone, E. L. Venturini, and P. M. Richards in *Electronic Structure and Properties of Hydrogen in Metals*, Edited by P. Jena and C. B. Satterthwaite (Plenum Press, New York, 1983) pp. 169.

[22] K. W. Jacobsen, J. K. Nörskov, and M. J. Puska, Phys. Rev. B **35**,7423 (1987).

[23] Y. Fukai and H. Sugimoto, Adv. Phys. **34**, 263 (1985); and references therein.

CHAPTER 3

MODELING THE SPECIFIC HEAT OF YH_2

3.1 Introduction

Knowledge of the specific heat of metal hydrides and in particular the partial molar entropy $\overline{S}_H$, enthalpy $\overline{H}_H$, and hydrogen chemical potential μ_H provide valuable insight into the hydrogen interactions. The heat capacity of metal hydrides generally contain anomalies which may be ascribed to various effects such as compositional changes and/or crystal phase transitions [1,2,3,4] upon hydrogen loading, variations in site occupation and location of the hydrogen sublattice, hydrogen-hydrogen interactions [2], Jahn-Teller effects [5] and magnetic effects [6,7]. In general, these anomalies show up as spikes in the heat capacity near the critical temperature and provide valuable thermodynamic information and insight into the hydrogen-metal and hydrogen-hydrogen interactions [8].

One may also obtain information concerning changes in the electronic structure from low temperature heat capacity studies. The addition of hydrogen into a metal lattice introduces a perturbing potential to the metal atoms which causes a rearrangement of electrons due to the extra proton and electron of the hydrogen atom. New electronic levels are introduced which modify the density of states of the pure host metal. At low temperatures, these modification may be probed by measuring the electronic contribution to the heat capacity which is a function of the density of states at the Fermi level.

In principle if the potential energy surface for the hydride where known with reasonable accuracy one could solve the equations of motion to obtain the phonon density of states, or frequency distribution, $g(\omega)$. A phonon being a vibrational quanta of energy $\hbar\omega$. For a constant volume system, the contribution of lattice vibrations to the specific may be be found as follows [9]:

$$C_v = k_B \sum_j \int \left(\frac{\hbar\omega}{2k_BT}\right)^2 \operatorname{csch}^2\left(\frac{\hbar\omega}{2k_BT}\right) g_j(\omega) d\omega \tag{4}$$

where k_B is Boltzmann's constant, $\hbar$ is Plank's constant divided by 2π, T is the absolute temperature and $g_j(\omega)$ is the frequency distribution of the j^{th} branch. The total frequency distribution may also be given as a sum over the number of branches: $g(\omega) = \sum_j g_j(\omega)$ where $j = 1, 2, \ldots, 3p$ with p being the number basis atoms per unit cell. For p atoms in the basis there are 3 acoustic branches and $3(p-1)$ optical branches. The difficulty in calculating the heat capacity by Eq. 4 is the determination of a reliable potential energy surface which adequately describes the M-M, M-H, and H-H interactions. A model which has met with reasonable success has been developed by Slaggie [10]. Here, nearest neighbor interactions for the metal-hydrogen and metal-metal interactions along with nearest and next nearest neighbor hydrogen-hydrogen interactions are treated in the central force approximation, i.e., bond bending or angular forces are ignored. Use of this model is hampered by the need for force constants; determined experimentally from inelastic neutron scattering data. Further, for non-stoichiometric hydrides where the hydrogen location is unknown, one must resort to a time consuming statistical description of the the site occupancy involving weighted distributions over the available sites.

Developing simpler models for the heat capacity involving less experimental data allows us to take advantage of the large mass difference between the hydrogen and metal atoms. Because of this difference, the motion of hydrogen and metal atoms are only weakly coupled. As such, the various branches may be decoupled into separate

metal and hydrogen branches. The hydrogen contribution to the heat capacity would then be calculated from Eq. 4 by summing only over optical branches resulting from the hydrogen atoms.

3.2 Model formulation

The total heat capacity of the hydride will be the sum of the acoustical and optical mode phonon contributions as well as electronic and configurational effects. If the separation between contributions is large the heat capacity contributions resulting from hydrogen in a transition metal may be modeled as [1]:

- Optical vibrations resulting from the presence of hydrogen.
- Changes in acoustical modes of the metal due to the elastic strain field on the metal lattice.
- Shifts in the density of states near the Fermi energy resulting from the additional electrons in the conduction band.
- Configurational effects due to varying interstitial site occupancy by the hydrogen atoms. Models usually include an additional term accounting for differences between C_p and C_v. This term is needed since heat capacity experiments are usually performed at constant pressure while theoretical studies are based on constant volume systems.

Deconvoluting the total heat capacity into the above contributions allows the separation of the partial molar heat capacity of hydrogen in the hydride. The heat capacity measurements [11] performed on $YH(D)_2$ between 5 K and 350 K [11] will be used to investigate hydrogen induced contributions to the total heat capacity. Here, configurational contributions caused by multiple site occupancy, as discussed in Chapter 2, will be included. Therefore, and additional term, C_v^{conf}, will be added to

the deconvolution of the total heat capacity of the dihydride. Following the notation of Moss *et al.* [12] for ScD_2

$$C_p = C_v^{l(a)} + C_v^{l(o)} + C_v^e + C^d + C_v^{conf} \tag{5}$$

where the first two terms are lattice contributions from the acoustical and optical modes respectively, the third term is the electronic contribution, the fourth is the dilation term and the last term is the configurational contribution due to multiple site occupancy.

3.2.1 Acoustical Contribution: $C_v^{l(a)}$

The heat capacity resulting from the acoustical modes may be developed in terms of the Debye model. This model successfully predicts the T^3 behavior at low temperatures as well as the high temperature Dulong-Petit behavior. For this reason the Debye model has been extensively used to predict the lattice contributions at intermediate temperatures. In principle there are only 3 acoustical branches which are possible. Thus for metal hydrides with more than one metal atoms per unit cell, one usually includes the optical modes by an Einstein model (See section 3.2.2). The acoustical contribution to the heat capacity resulting from the metal lattice, which in the Debye model is given by:

$$C_v^{l(a)} = 9R\left(\frac{T}{\Theta_D}\right)^3 \int_0^{\Theta_D/T} \frac{x^4 e^x}{(e^x - 1)^2} dx \tag{6}$$

where $x = \hbar\omega/k_B T$, Θ_D is the Debye temperature, and R is the gas constant. The corresponding Debye temperature may be related to the average sound velocity of the three acoustical modes by

$$\Theta_D = \frac{h}{k_B}\left(\frac{3p}{4\pi V_{cell}}\right)^{\frac{1}{3}} v_m \tag{7}$$

where V_{cell} is the primitive cell volume, p is the number of atoms per primitive cell contributing to the acoustical modes, and v_m is the mean velocity of sound through the solid. For a polyatomic solid, the mean sound velocity may be described in terms of the the longitudinal, v_l and transverse or (shearing) v_t sound velocities [2] where

$$v_m = \left(\frac{2}{3v_t^3} + \frac{1}{3v_l^3} \right)^{-\frac{1}{3}}. \tag{8}$$

This averaging basically assumes that one can model the crystal as an isotropic solid in the continuum limit with one longitudinal branch and two degenerate transverse branches.

The experimental acoustical transverse and longitudinal sound velocities have been measured for polycrystalline $YH_{1.93}$ by Beattie *et al.* [13] in the temperature range range 80 K $\leq$ T $\leq$ 300 K. Both velocities exhibit two regimes where the sound velocity varies linearly with temperature with a transition near 230 - 240 K. This is similar to that found for $ScH_{1.99}$ and $ErH_{1.81}$. While this change in slope of the acoustical velocities with temperature indicates that a phase transition may be responsible, no conclusive evidence has been found from neutron diffraction experiments [14]. Further, changes in the elastic constants and/or long range ordering of the crystallites could be responsible for these changes [13]. However, the abrupt changes seen in the slopes of the longitudinal and transverse sound velocities are more likely explained by the decrease in the order of the metal lattice due to O site occupancy as observed in the high energy spectrum of the optical absorptivity experiments [14] discussed in Chapter 2. The acoustical longitudinal and transverse sound velocities where approximated by linear fits in the respective temperature ranges. The parameters are given in Table 2. The effect of temperature on Θ_D, given by Eq. 7, is not only influenced by the changes in the acoustical sound velocities but also through the changes in the volume of the crystal. Generally, an increase in temperature leads

Table 2: Linear fits to experimental [13] sound velocities for polycrystalline $YH_{1.93}$ as a function of temperature. Sound velocities are given as: $v_i = a_i - b_i T$ where $i = l, t$ for the longitudinal and transverse acoustical branches. Velocities are given in units of 10^5 cm/s and temperature in K.

Temperature	longitudinal		transverse	
(K)	a_l	b_l	a_t	b_t
80 - 230	6.321	$1.818 \cdot 10^{-4}$	3.719	$1.272 \cdot 10^{-4}$
240 - 300	6.403	$5.406 \cdot 10^{-4}$	4.219	$2.154 \cdot 10^{-3}$

to an increase in volume and a decrease in the acoustical sound velocities. Volume increases due to temperature can be described in terms of the the volume expansivity of the solid β, where

$$\beta \equiv \frac{1}{V_{cell}} \left(\frac{\partial V_{cell}}{\partial T} \right)_P \tag{9}$$

For crystals of cubic symmetry, $\beta = 3(\partial a/\partial T)_P/a$, where a is the lattice constant. Equation 9 gives

$$a = a_0 \exp\left(\int_0^T \alpha(T) dT \right) \tag{10}$$

where a_0 is the lattice constant at 0 K and α is the thermal coefficient of linear expansion given by: $\alpha(T) = \beta/3$. For YH_2, variations in the lattice constant with temperature are expected to be small as evidenced by the phase stability of $YH_{2\pm\delta}$ over a considerable range of disorder δ. In recent neutron diffraction experiments, Goldstone *et al.*[15] confirmed this, observing a lattice constant of 5.1947 Å at 15 K and 5.2037 Å at 300 K. This small, 0.2% change in the lattice constant suggests that the Debye temperature is not a strong function of the lattice constant. The thermal coefficient of linear expansion used in Eq. 10 was based upon experimental

results for $YH_{1.93}$ [21] in the temperature range 260 to 899 °C. Thus, although the optical properties of YH_2 are strongly affected by hydrogen disorder [14], the effect of concentration on the thermal expansion coefficient is assumed to be negligible. This H-concentration independence is supported by low temperature neutron diffraction experiments, Weaver *et al.*[14], for YH_x in the range $1.47 \leq x \leq 1.96$, where the lattice constant was found to approximately independent of hydrogen concentration. The temperature dependence for α, was thus fit to experimental results for $YH_{1.93}$ [21], where we find

$$\alpha(T) = 2.224 \times 10^{-6} + 1.205 \times 10^{-8} T \qquad (K^{-1}) \tag{11}$$

with a correlation coefficient ≈ 1. Substituting this into Eq. 10 and retaining only the first Taylor series expansion term for the exponential yields:

$$a(T) \cong 5.1946(1 + 2.224 \cdot 10^{-6} T + 6.026 \cdot 10^{-9} T^2). \tag{12}$$

where the value of a_0 was taken from neutron diffraction studies at 11 K [15].

3.2.2 Hydrogen Contribution: $C_v^{l\,(o)}$

Inelastic neutron scattering results for the dihydride and dideuteride [16], reveal well separated acoustical and optical peaks via time of flight spectroscopy. Thus, to a good approximation, the acoustical metal modes and the optical hydrogen modes may be treated separately, i.e., weak coupling between the modes. We will thus consider the vibration of the hydrogen atoms as independent particles vibrating in a harmonic potential well.

As discussed in Chapter 2, a significant fraction of hydrogen YH_2 ocupies "high energy" octahedral sites in YH_2 even at low temperatures [17]. Thus, a significant contribution to the hydrogen heat capacity will be vibrational modes resulting from

O site occupation. The coupling between H atoms at O and T sites depends on H-H interactions, and dominates the shift in frequency distributions, but in the present study, it is assumed that the hydrogen atoms in T and O sites vibrate independently. The differences in frequency and energy between O and T sites are assumed to be solely due to differences in short range M-H interactions which arise from bonding states [18]. Ignoring H-H interactions and, for now, H-exchange between sites, the total heat capacity of the hydrogen sublattice is approximated as

$$C_v^{l(o)} = x_O C_v^{H_O} + 2x_T C_v^{H_T} \tag{13}$$

where x_O and x_T are the fraction of occupied octahedral and tetrahedral sites respectively and $x = x_O + 2x_T$ is the number of hydrogens per metal atom. The subscripts on H indicate the hydrogen site.

Following the neutron scattering results discussed previously, the heat capacity of a hydrogen atom in any particular site is modeled as a harmonic Einstein oscillator. Thus for example, the heat capacity of a hydrogen atom at a T site is given by:

$$C_v^{H_T} = 3R\left(\frac{\Theta_E}{T}\right)^2 \frac{e^{\Theta_E/T}}{(e^{\Theta_E/T}-1)^2} \tag{14}$$

where Θ_E is the Einstein temperature, $\Theta_E = \hbar\omega_T/k_B$ where ω_T is the circular vibrational frequency of hydrogen in a tetrahedral site. A similar equation exists for hydrogen at an O site.

The Einstein model, on which Eq. 14 is based, requires that the optical part of the hydrogen frequency distribution is represented by a Dirac delta function. Time of flight spectra, however, usually show Gaussian type distribution dispersion rather than a pure Delta function which may be attributed to H-H interactions as was shown for $CeD_{2.12}$ [19]. Equation 14 may be improved by using a Gaussian function for the optical mode frequency distribution as in the Slaggie model [10], however, for YH_x

(and similar hydrides), theses contributions appear to be small [15]. Thus, Eq. 14 should provide reasonable results.

Recent inelastic neutron scattering experiments [15] on $YH_{1.54}$ and $YH_{1.97}$ at 600 K revel a single peaked frequency distribution for the optical branch at 118 meV. At this temperature, O site occupation is negligible [15] and therefore, if H-H interactions between neighboring tetrahedral sites was significant one would expect broadening of the frequency distribution as hydrogen concentrations increase. That such broadening did not occur, indicate that H-H interactions between nearest neighbor T sites is negligible. At low temperatures where O sites are occupied, a shoulder occurs at the high energy side of the T site peak; this shoulder is caused (presumably) by hydrogen T and O site interactions [15,17,20]. The T site frequencies are 117 meV with a shoulder at 127 meV and the O site frequency occurs at 81 meV [15,17]. Thus, for use in Eq. 14, the T and O site Einstein temperatures were taken to be 1358 K and 940 K respectively [15,17].

3.2.3 Electronic Contribution: C_v^e

As in all conductors, the electronic conduction band contribution to the heat capacity is proportional to temperature, i.e.,

$$C_v^e = \gamma T. \tag{15}$$

We solve for γ from low temperature heat capacity data, e.g., Table 3 [11]. Since, at low temperatures, the heat capacity of the dihydride is approximately the sum of the yttrium lattice acoustical mode contributions and the electronic contribution, Eq. 15,

$$C_v(T \to 0K) \cong \gamma T + \frac{12\pi^4 p k_B}{5}\left(\frac{T}{\Theta_D}\right)^3. \tag{16}$$

Table 3: Low temperature experimental heat capacity values for YH_2 and YD_2 as taken from Flotow *et al.* [11] where heat capacity is in 10^{-3}cal/mol·deg and temperature is in K

YH_2		YD_2	
T	C_p	T	C_p
5.88	5.6	5.22	4.6
6.00	5.8	5.91	5.9
7.97	9.6	7.03	7.6
7.97	9.6	8.89	11.8
9.89	14.8	9.88	15.1
10.03	15.4	10.75	19.2

Table 4: Comparison of the coefficient of specific heat for YH_2 and limiting Debye temperatures calculated from the low temperature experimental heat capacity experiments [11]

Data set	$\gamma \cdot 10^4$ (cal/mol·deg^2)	Θ_D (K)
YH_2	6.52	376
YD_2	6.52	374

Values of γ and Θ_D can be found from low temperature heat capacity [11] data for YH_2 and YD_2 by a plot of C_v/T versus T^2. The corresponding values of γ and the limiting Debye temperatures are given in Table 4. The limiting value of the Debye temperature is relatively insensitive to isotopic substitution as is expected as the number of phonons excited at such low temperatures is small as compared to the acoustical phonons. This value of the limiting Debye temperature ($\sim$ 375 K) is identical with the value 375 K calculated from the acoustical sound velocities [13], and is probably more accurate than the value 340 K obtained from electrical resistivity studies, Daou *et al.* [22]

3.2.4 Dilation Contribution: C_v^d

As previously mentioned, a dilation term is included in the heat capacity estimations to take into account differences between experimentally determined constant pressure heat capacity and theoretically determined constant volume values. Thermodynamically, the dilation term [12] is

$$C^d = C_p - C_v = \frac{-T(\partial V/\partial T)_P^2}{(\partial V/\partial P)_t} = \beta^2 T V B_i \tag{17}$$

where V is the molar volume ($N_A a^3/4$ for an fcc lattice) and B_i is the isothermal bulk modulus which can be related to the adiabatic bulk modulus, B_a by the following [12]:

$$\frac{1}{B_i} = \frac{1}{B_a} + \frac{\beta^2 T V}{C_p}. \tag{18}$$

The adiabatic bulk modulus B_a may be calculated from elastic data, where [12]

$$B_a = \frac{M}{V}(v_l^2 - \frac{3}{4}v_t^2) \tag{19}$$

where M is the molecular weight of the the atoms contributing to the acoustical mode and v_l, v_t and β are the longitudinal and transverse speed of sound and thermal expansion coefficient previously given.

3.2.5 Configurational Contribution: C_v^{conf}

Various models proposed for O site occupancy do not predict the anomalous decrease in O site occupation with increasing temperature [23]: they predict that the "high energy" O site is occupied only at high temperature and not at all at 0 K. Short of calculating the cause of the small H-H interactions which cause the anomaly, one needs to now x_0 *a priori* in order to calculate the heat capacity. Specifically, a configurational heat capacity occurs due to the random redistribution of hydrogen over

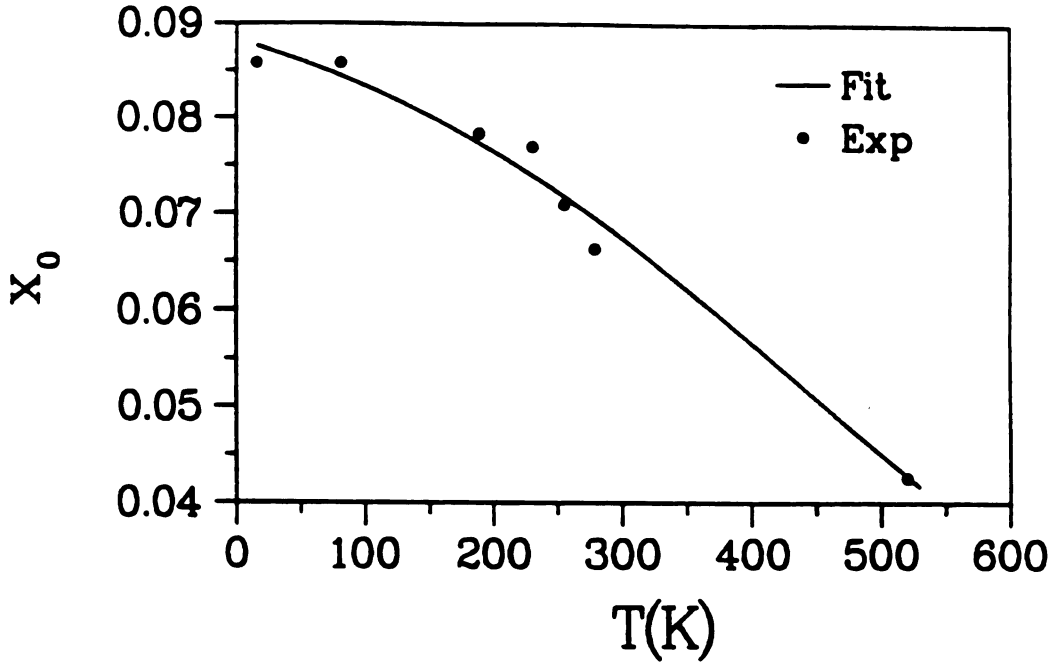

Figure 3: Experimental octahedral site occupancy in YH_2 determined from INS [15] experiments. The solid line representing the fit to the experimental data as given by Eq. 3.

the O and T sublattices. Prior attempts at determining the O site occupancy from equating the chemical potentials of hydrogen in the two sites have been unsuccessful in matching the experimental results [24]. Thus, x_O is taken directly from INS experiments [15] fit to the following functional form:

$$x_O = \frac{a}{1 + b\exp(T/c)} \tag{20}$$

where $a = 0.09766$, $b = 0.1063$ and $c = 208.9$. The experimental values for x_0 along with that predicted from Eq. 20 is shown in Figure 3. Neglecting H-H interactions,

as previously discussed, the internal energy of the hydrogen atoms, at $x = 2$, is given by

$$U_H = x_O U_{H_O} + 2x_T U_{H_T}. \tag{21}$$

The heat capacity for the hydrogen sublattice is defined as:

$$C_v^H = \left(\frac{\partial U_H}{\partial T}\right)_V. \tag{22}$$

Here, U_H and C_v^H are for the total hydrogen sublattice including both T and O occupation. Substituting Eq. 21 into 22 yields:

$$C_v^H = x_O C_v^{H_O} + 2x_T C_v^{H_T} + (U_{H_O} - U_{H_T})\frac{dx_O}{dT} \tag{23}$$

where $U_{H_O} - U_{H_T}$ is the energy difference between the O and T sites. Equation 23 may be conveniently separated into vibrational and configurational contributions where

$$C_v^H = C_v^{l(o)} + C_v^{conf} \tag{24}$$

the configurational contribution being given by

$$C_v^{conf} = (U_{H_O} - U_{H_T})\frac{dx_O}{dT} \tag{25}$$

and the optical contribution due to the hydrogen vibrations being previously defined by Eq. 13.

One expects the site energy difference to be relatively insensitive to variations in temperature due to the almost constant lattice constant. Thus to a good approximation, $U_{H_O} - U_{H_T}$ is taken as a constant. Electron spin resonance (ESR) studies [25] performed on $YH(D)_2$ have determined the energy difference between the T and O

sites by a fit to the following parameter

$$B = \exp[(U_{H(D)_T} - U_{H(D)_O})/k_B T_f] \tag{26}$$

Using a mean field approximation for the hydrogen sublattice motion [25], the corresponding values of B were found to be 0.0040 and 0.0025 for H and D respectively [25]. Further, the inclusion of H-H interactions did not significantly affect the results [25]. In Eq. 26, T_f is the "freezing" temperature of the hydrogen sublattice and was assumed to be that at which the mean residence time for hydrogen at a particular site was one minute. The value of T_f used by Venturini was approximated from the proton NMR results for ScH_2 were $T_f = 150\ K$. Rather than using the above value for T_f, we have extrapolated the proton NMR data [26] for $YH_{1.98}$ and find a "freezing" temperature of 114 K. Using this T_f and the value of B for H and D [25], the site energy differences, $U_{H(D)_O} - U_{H(D)_T}$ was found to be 54 and 59 meV for H and D respectively, as opposed to the values of 71 and 78 meV given by Venturini with the value of 150 K for T_f.

3.3 Results and Discussion

The above model may tested by comparing the heat capacity as predicted by Eq. 5 to the experimentally determined heat capacity values [11]. The resulting comparison between experiment and theory is shown in Figure 4, along with the predicted contributions resulting from the metal lattice, Eq. 6, and the hydrogen sublattice contribution predicted from Eq. 24. The electronic and dilation terms are insignificant compared to these terms. As seen in Figure 4, reasonable agreement is obtained at high temperatures; however, the model significantly underestimates the low temperature values. This underestimation is easily seen in Figure 5 where the difference

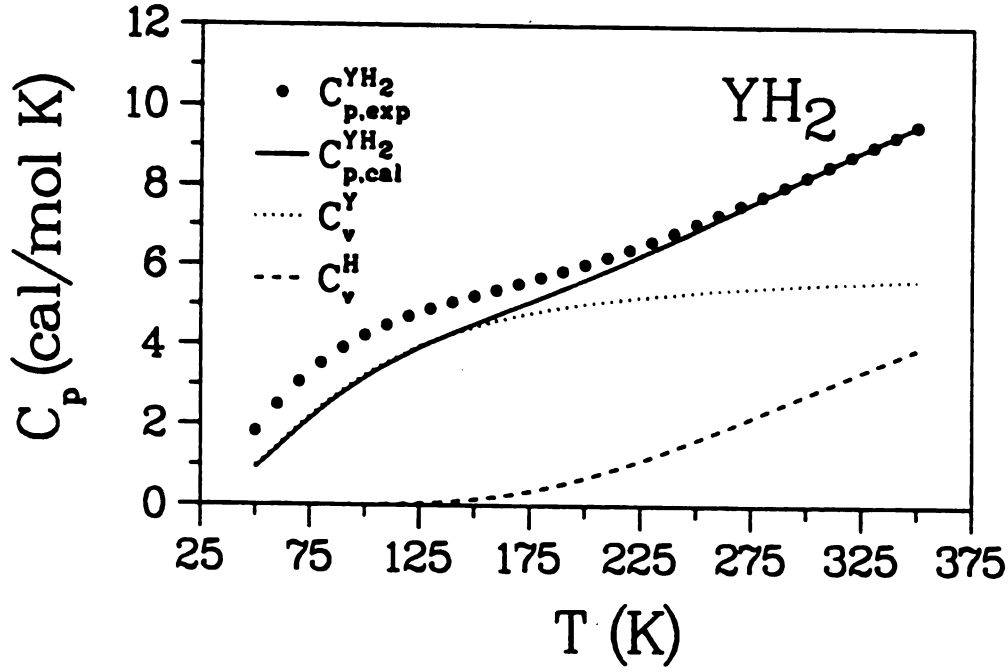

Figure 4: Comparison of experimental and theoretical predictions for the heat capacity of YH_2. Experimental values are taken for Flotow *et al.* [11].

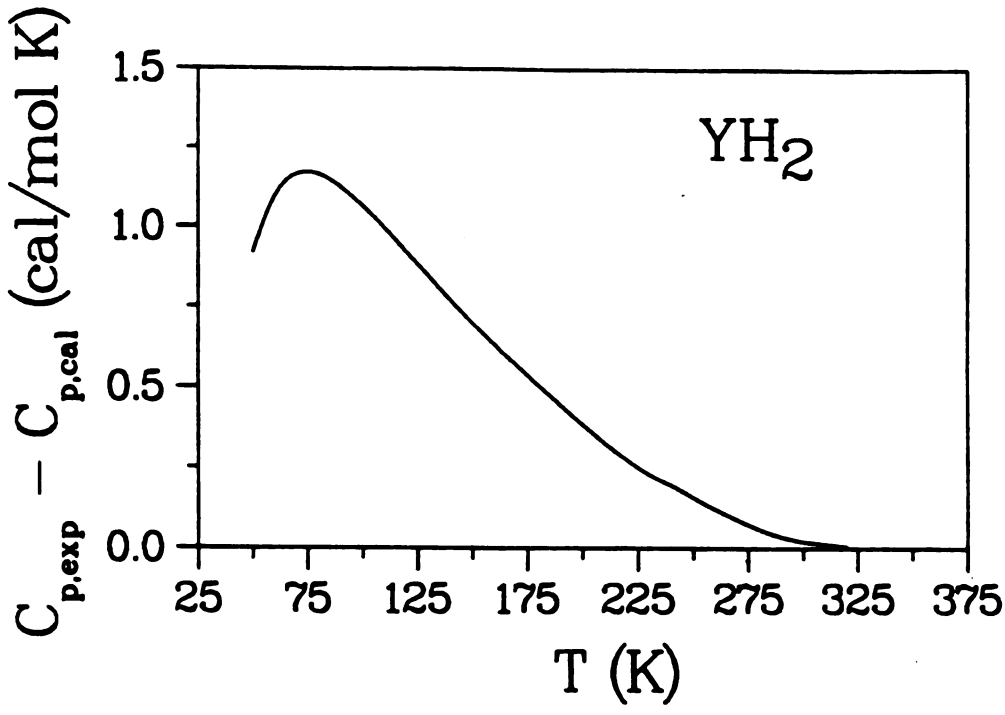

Figure 5: Error in the total heat capacity at constant pressure fo the YH_2 system compared to the experimental predictions

between the experimental and theoretical values are shown. The corresponding difference being as large as $\sim$ 1 cal/mol·deg at 75 K. Since the electronic and dilation terms contribute only minimally to the total heat capacity, the discrepancy must exist in the configurational, acoustical, or optical contributions, i.e., these are the only terms which can give rise to such a large discrepancy.

As seen from Figure 3, the configurational contribution resulting from the distribution of hydrogen atoms over the available tetrahedral and octahedral sites is a decreasing function of temperature. Thus, the configurational contribution predicted from Eq. 25 will always lead to a decrease in the total heat capacity. A major

question arises as to whether or not the experimentally predicted octahedral site occupancy is physically reasonable. By extrapolating from the NMR data [26] it is estimated to take $\sim$ 10 hr for a hydrogen atom to jump from one site to another at 90 K. Obviously, hydrogen motion is severely diffusion limited indicating that the O site occupancy may actually decrease as the temperature is lowered rather than maintaining a constant value as experimentally observed [25]. If this were the case, a positive contribution would result from the configurational heat capacity, though an estimate of this term is difficult due to the time needed for equilibriation of the sample. However, one would expect that at higher temperatures, experimental heat capacity measurements would be able to discern this effect if the rate of temperature ramping was varied. Similar results were observed in experimental conductivity measurements where samples where quenched from high temperatures thereby freezing in hydrogen atoms occupying octahedral sites [14].

In Figure 6 the optical contribution from the hydrogen sublattice resulting from Eq. 13 as well as the individual contributions from tetrahedral and octahedral occupancy are shown. With the vibrational frequency of the octahedral sites being less than the tetrahedral sites, the Einstein model gives a larger contribution resulting from octahedral site occupancy. However, the values shown in Figure 6 must be weighted by their corresponding occupational probabilities. Since octahedral site occupancy being such that $x_0 \ll x_T$, the actual contribution from the octahedral sites are small. If the octahedral site occupancy were to increase, a significant increase in the theoretical heat capacity would be observed; possibly accounting for the large discrepancy seen in Figure 5. Further, the present model does not take into account the hydrogen-hydrogen interactions. At high temperatures these effects are not expected to be important; however, at low temperatures these effects may become important. That this is significant, is seen in the INS experiments [25] which show an additional shoulder to the tetrahedral peak towards higher energy, i.e., 127 meV. This gives an

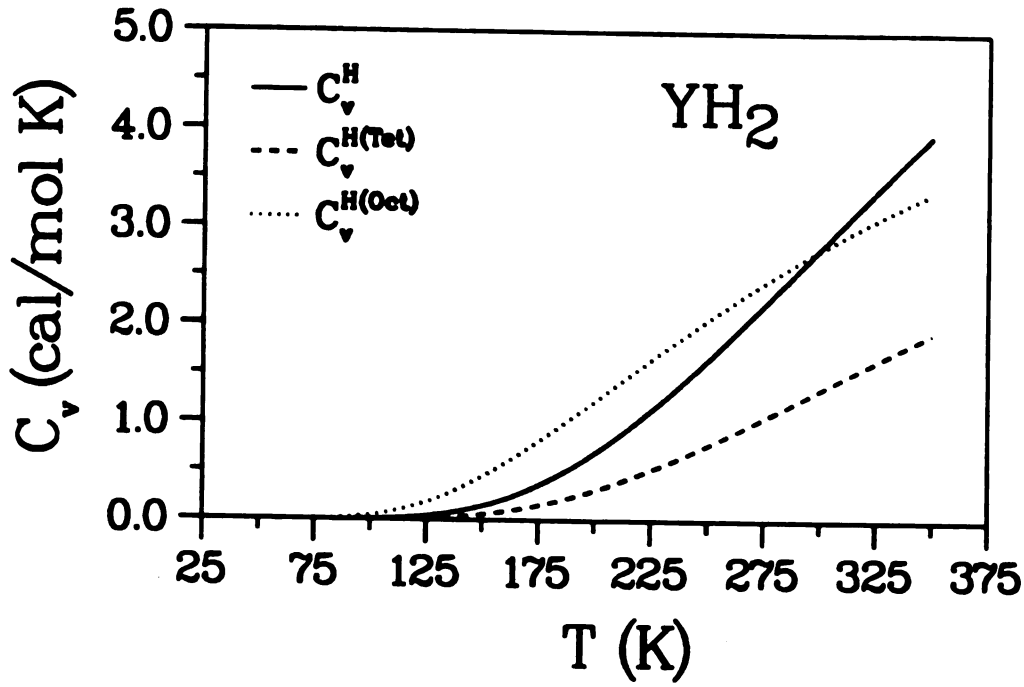

Figure 6: Hydrogen sublattice contributions resulting from optical vibrations. Vibrational frequencies are taken as 117 meV and 81 meV for the tetrahedral and octahedral sites.

indication that the low temperature vibrational motions between hydrogen atoms on different sites are coupled. To account for these interactions is beyond the scope of the present work and could account for the discrepancy between the present model and experiment.

A further contribution to the heat capacity at low temperatures results from the the acoustical vibrations of the metal lattice. The results shown in Figure 4 are for Θ_D values taken from experimental sound velocity measurements which should provide a reasonable approximation to the acoustical contribution within the Debye approximation. In these experiments, a discontinuity was observed in the longitudinal and transverse sound velocities at low temperatures indicating that the Debye approximation may break down in this region. Further, if the octahedral site occupancy does in fact decrease with increasing temperature then one must take into account heat capacity contributions resulting in changes of the metal lattice entropy where the entropy increases (decreases) when a proton enters a tetrahedral (octahedral) site [23,15]. These effects are beyond the Debye model as well as the allowance for hydrogen-hydrogen interactions.

3.4 summary

In the present chapter it has been shown that a simple model taking into account of the major contributions to the heat capacity works rather well at high temperatures, i.e., $T > \Theta_D$. However, the model severely underestimates the heat capacity at low temperatures. Various reasons for the discrepancy have been presented which revolve around the hydrogen and metal lattice vibrational contributions. From the present results, it is apparent that further experimental effort is needed in order to actually resolve the discrepancy. Specifically, in order to explore the configurational contributions we have suggested an experiment which would be able to determine the significance of this term.

LIST OF REFERENCES

[1] R. Heibel, H. Wollenberger and H. Zabel, J. Less-Common Metals **57**, 177 (1978).

[2] T. Ito, B. J. Beaudry and K. A. Gschneidner, J. Less-Common Met. **88**, 425 (1982).

[3] B. Yates, G. H. Wostenholm and J. L. Bingham, J. Phys. C. **7**, 1769 (1974).

[4] R. L. Crane, S. C. Chattorag and M. B. Strope, J. Less-Common Met. **25**, 225 (1971).

[5] A. C. Switendic J. Less-Common Met. **101**, 191 (1984).

[6] M. Drulis, J. Opyrchal and W. Borkowska, J. Less-Common Met. **101**, 211 (1984).

[7] K. Bohmhammel, G. Wolf, G. Gross and H. MÕdge, J. Low Temperature Phys. **43**, 521 (1980).

[8] Z. Biegański and B. Staliński, J. Less-Common Met. **49**, 421 (1976).

[9] N. W. Ashcroft and N. D. Mermin, *Solid State Physics* (Saunders College, Philadelphia, 1976).

[10] E. L. Slaggie, J. Phys. Chem. Solids **29** 923 (1968).

[11] H. E. Flotow, D. W. Osborne and K. Otto, J. Chem. Phys. **36**, 866 (1962); and references therein.

[12] M. Moss, P. M. Richards, E. L. Venturini, J. H. Gieske, and E. J. Graeber, J. Chem. Phys. **84**, 956 (1986).

[13] A. G. Beattie, J. Appl. Phys. **43**, 3219 (1972).

[14] J. H. Weaver, R. Rosei and D. T. Peterson, Phys. Rev. B **19**, 4855 (1979).

[15] J. A. Goldstone, J. Eckert, P. M. Richards, and E. L. Venturine, Solid State Comm. **49**, 475 (1984).

[16] J. J. Rush, H. E. Flotow, D. W. Connor and C. L. Thaper, J. Chem. Phys. **43**, 3817 (1966).

[17] J. A. Goldstone, J. Eckert, P. M. Richards and E. L Ventruini, Phisca B **136**, 183 (1986).

[18] Y. Fukai and H. Sugimoto, J. Phys. F. **11**, L137 (1981).

[19] C. J. Glinka, J. M. Rowe, J. J. Rush, G. G. Libowitz and A. Maeland, Solid State Comm. **22**, 541 (1977).

[20] J. A. Goldstone, E. L. Venturini and P. M. Richards in *Electronic Structure and Properties of Hydrogen in Metals*, Edited by P. Jena and C. B. Satterthwaite (Plenum Press, New Yourk, 1983) pp. 169.

[21] G. G. Libowitz, *The solid state chemistry of binary metal hydrides* (Benjamin, New York, 1965).

[22] J. N. Daou, A. Lucasson, P. Vajda, and J. P. Burger, J. Phys. F **1**, 2983 (1984).

[23] J. D. Patterson and P. M. Richards, J. Less-Common Metals **138**, 281 (1988).

[24] K. M. Glassford and R. E. Buxbaum, AIChE Student Conference, Ann Arbor Michigan, 1989 (unpublished).

[25] E. L. Venturini, J. Less-Common Metals **74**, 45 (1980).

[26] D. L. Anderson, R. G. Barnes, T. Y. Hwang, D. T. Peterson and D. R. Torgeson, J. Less-Common Met. **73**, 243 (1980).

CHAPTER 4

H POTENTIAL ENERGY SURFACE IN YH_2

4.1 Introduction

The present chapter discusses various empirical models used in describing the potential energy surface of hydrogen in transition metal hydrides. The potential energy surface provides valuable insight into the diffusion mechanism as well as furnishing valuable information concerning the anomalous occupation of octahedral site occupation in the yttrium dihydride system. In Section 4.2, a general discussion of the homogeneous electron gas model used in calculating the hydrogen potential energy surface is presented. A brief introduction into density functional theory which forms the basis for the present model along with modifications due to the metal atom cores is also given. Section 4.4, discusses various correction terms to the embedding energy for hydrogen in a homogeneous electron gas. Particularly important here are methods involving first order perturbation theory as well as corrections due to the one electron potential and hybridization effects due to the choice of the effective medium.

4.2 Jellium Model

A starting point for many theoretical treatments of hydrogen in metals, is the so called jellium model which considers the impurity atom embedded in a homogeneous electron gas [5]-[5].The pure metal host is envisioned as a lattice of metal ions immersed in a sea of valence electrons providing a classical picture of conduction electrons in

metals. Introducing a hydrogen atom (a proton and electron) into the metal causes a redistribution of the valence electrons surrounding the impurity due to Coulomb interactions between the proton and the sea of electrons and positive metal atom cores. The jellium model treats the interaction between the valence and metal atom cores by effectively smearing out metal cores over the volume of the crystal. The valence electrons are similarly distributed over the crystal, providing a homogeneous electron gas density and charge neutrality. The homogeneous background charge distribution is

$$n_0 = \frac{Z_v}{\Omega_0} \tag{27}$$

where Z_v is the metal ion valence, and Ω_0 is the atomic volume. The density of this homogeneous electron gas is often described in terms of an electron spacing parameter, r_s, where $n_0 = 3/(4\pi r_s^3)$. The electron spacing parameter, is effectively the radius of the sphere occupied by a single electron and is a measure of the distance between valence electrons. Form metals, r_s typical ranges from 2 to 6 a.u., where 1 a.u. = 0.5292 Å and is the atomic unit of length. In this range of r_s values the valence electrons are approximately spaced a half to one lattice constant from each other for typical metals. To solve for the interaction, one solves Schrödinger's wave equation for the electron gas density self-consistently using the local density function formalism of Hoenberg-Kohn-Sham [6] (hereafter referred to as HKS). The solution yields the energy and the impurity induced or "displaced" electron density of the hydrogen atom at the chosen value of r_s. This "displaced" electron density, is the difference between the electron density of the impurity-jellium system and n_0; it describes in a sense, the screening of the impurity atom due to the charge of the jellium.

4.2.1 Density functional theory

Since density functional theory plays a pivotal role in calculating the displaced electron density and embedding energy of the hydrogen atom in a homogeneous electron gas, it will be reviewed here briefly. Reference [7] is recommended for a fuller review of homogeneous and inhomogeneous electron gas methodology. In the HKS formalism the total energy of a system of electrons of density $n(\mathbf{r})$ is given by [7]

$$E[n(\mathbf{r})] = T_0[n(\mathbf{r})] + \int n(\mathbf{r}) V_{ext}(\mathbf{r}) d\mathbf{r} + \frac{1}{2} \int \int \frac{n(\mathbf{r}) n(\mathbf{r}')}{|\mathbf{r} - \mathbf{r}'|} d\mathbf{r} d\mathbf{r}' + E_{xc}[n(\mathbf{r})], \quad (28)$$

where the brackets denote density functionals, i.e., functions of the electron density. The first term is the kinetic energy of non-interacting electrons of density $n(\mathbf{r})$, the second term is the interaction of the electron density with the external potential ($V_{ext}(\mathbf{r}) = -1/r$ for a hydrogen impurity), the third term is the average electrostatic Hartree energy of the electrons, and $E_{xc}[n(\mathbf{r})]$ is the exchange correlation energy. The variational principle states [7] that the true ground state electron density is that which minimizes $E[n(\mathbf{r})]$. The resulting single particle Schrödinger like equations in atomic units ($\hbar = m = e = 1$) are given by

$$-\frac{1}{2}\nabla^2 \psi_i(\mathbf{r}) + V_{eff}[n(\mathbf{r}), \mathbf{r}] \psi_i(\mathbf{r}) = \epsilon_i \psi_i(\mathbf{r}) \quad (29)$$

where V_{eff} is the effective one electron potential. The electron density is obtained by summing over the occupied pseudo-orbitals where

$$n(\mathbf{r}) = \sum_i^{occ} \psi_i^*(\mathbf{r}) \psi_i(\mathbf{r}). \quad (30)$$

The effective one electron potential, V_{eff}, is the sum of the electrostatic potential, $\phi(\mathbf{r})$, and the and exchange-correlation potential, $V_{xc}[n(\mathbf{r})]$. The one electron effective

potential [6] is given by:

$$V_{eff}[n(\mathbf{r}),\mathbf{r}] = \phi(\mathbf{r}) + V_{xc}[n(\mathbf{r})] \tag{31}$$

were the electrostatic potential is given by:

$$\phi(\mathbf{r}) = V_{ext}(\mathbf{r}) + \int \frac{n(\mathbf{r}')}{|\mathbf{r}-\mathbf{r}'|} d\mathbf{r}'. \tag{32}$$

The difficulty in solving Schrödingers wave equation lies in evaluating the exchange correlation energy, E_{xc} for which no functional form exists which can describe this term explicitly. In order to evaluate this term one usually turns to the local density approximation or LDA, in which the electron density at a given position is an average of local electron density surrounding this point and is a slowly varying function. Thus, the exchange-correlation potential is given by:

$$V_{xc}[n(\mathbf{r})] \approx \frac{d(n(\mathbf{r})\epsilon_{xc}[n(\mathbf{r})])}{dn(\mathbf{r})} \tag{33}$$

where ϵ_{xc} is the exchange-correlation energy density. There are many approximations for ϵ_{xc} in the literature; the Monte Carlo calculations of Ceperley and Alder [8] and parameterized by Vosko, Wilk and Nusiar [9] is considered to be the most accurate of these [10].

The major advantage of the homogeneous electron gas approximation lies in the spherical symmetry of Eq. 29 for the embedded atom-host system. The displaced electron density is $\Delta n(r) = n(r) - n_0$, where $n(r)$ is the electron density of the atom-host system calculated from the HKS equations at self consistency. The great simplifications that result are analogous to those in the Schrödinger wave equation for atomic wave functions [3]. Figure 7 illustrates the functional form of $\Delta n(r)$ for a typical value of $r_s = 3$ a.u. (see Section 5.4 for details). The energy needed to embed

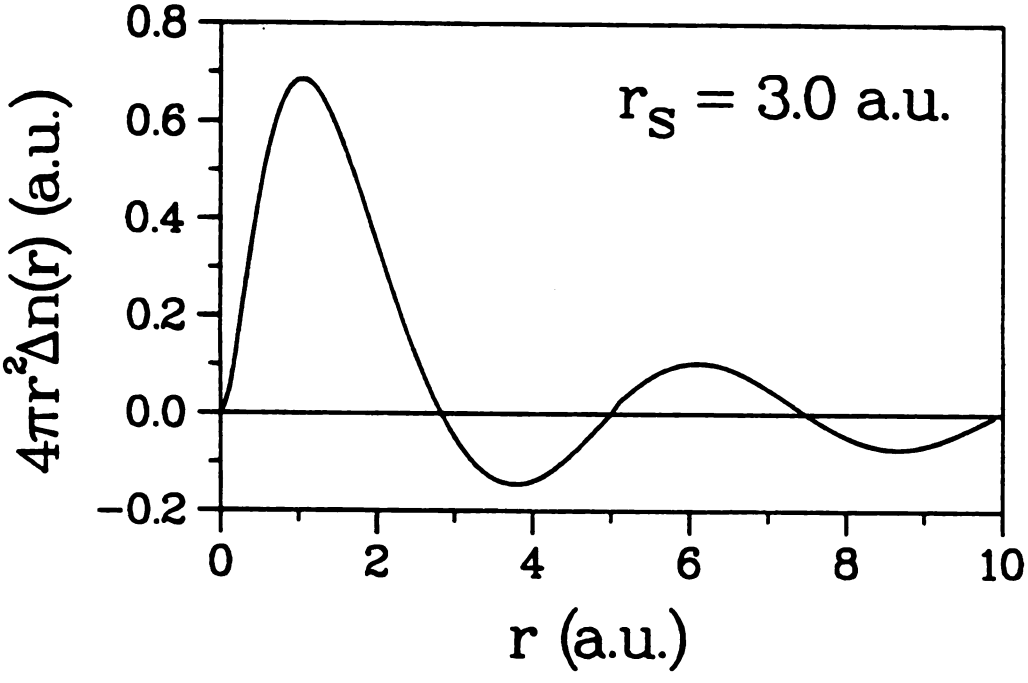

Figure 7: Hydrogen included electron density in a homogeneous electron gas

the impurity atom in the homogeneous electron gas is now calculated *via*

$$\Delta E^{hom}(n_0) = E[\Delta n(\mathbf{r}) + n_0] - E[n_0] - E[n_H(\mathbf{r})], \tag{34}$$

where $n_H(\mathbf{r})$ is the free atom electron density. It should be noted that the homogeneous embedding energy, ΔE^{hom}, is not applicable to the HKS formalism, i.e., it is only the individual terms appearing in Eq. 34, used in calculating ΔE^{hom}, that are valid. The homogeneous embedding energy, as calculated by Eq. 34, need only be calculated once for any given atom over the desired range n_0. In fact, $\Delta E^{hom}(n_0)$ has been calculated for a variety of atoms [3,11,12] for values of n_0 spanning the metallic density range. The hydrogen embedding energy in a homogeneous electron gas is shown in Figure 8. From this figure it is simple to understand why the metal atoms expand around the hydrogen atom upon their incorporation into the lattice. As the metal atoms move away from the embedding site, the electron density which the impurity atom experiences decreases thus leading to a net stabilization. Although other effects are involved, much can be learned from this simple picture. Various features of this curve have been discussed by Nørvosk [5] and Stott and Zaremba [2].

4.3 Spherical Solid Model

The jellium model appropriately treats the hydrogen potential to infinite order, yet neglects the interaction between the displaced electron density and ion cores. However, if the potential caused by the metal cores is slowly varying, then this effect on the potential may be considered in perturbation theory. To explicitly account for the host ion-impurity interactions directly, the external potential, $V_{ext}(\mathbf{r})$, given in Eq. 28 and 32 would need to be replace by

$$V'_{ext}(\mathbf{r}) = V_{ext}(\mathbf{r}) + \hat{V}_{ion}(\mathbf{r}) \tag{35}$$

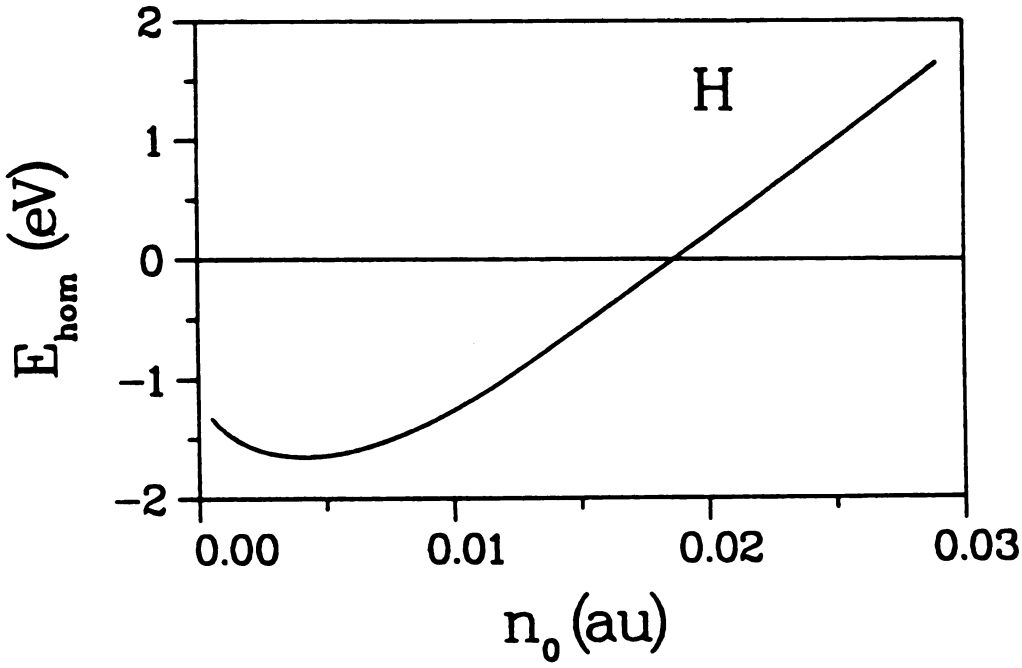

Figure 8: Embedding energy of H in a homogeneous electron gas

where $\hat{V}_{ion}(\mathbf{r})$ is the total ionic potential (non-local) resulting from the metal atom cores. Introducing the ions explicitly increases the complexity of the problem tremendously. The major difficulties lie in the fact that the wave functions are periodic and must therefore obey both Bloch's theorem and "non-local" behaviors caused by the ion cores. "Non-locality" here indicates that an s electron will see a different core-induced potential than say, a p electron. Equation 35 has an assumption too, that core electrons are independent of their specific environment, i.e., core electrons have the same properties in the atomic case as in the solid. This, so called "frozen core approximation" is largely due to the fact that core electrons play a small role in the cohesion of solids. Thus, the total ionic potential is given by

$$\hat{V}_{ion}(\mathbf{r}) = \sum_{l} \hat{v}_{ps}(\mathbf{r} - \mathbf{R}_l) \tag{36}$$

where $\hat{v}_{ps}(\mathbf{r})$ is the non-local pseudopotential from a single metal atom core. The external potential, $V'_{ext}(\mathbf{r})$, defined by Eq. 35, would be used in the self consistent solution of the HKS equations. However, solving for the energy in this way would of course be equivalent to solving the many-body problem.

The spherical solid model [13] modifies Eq. 36 by replacing the non-local pseudopotentials by local pseudopotentials involving a spherical a average over $\hat{V}_{ion}(\mathbf{r})$. Thus,

$$\hat{V}_{ion}(\mathbf{r}) \rightarrow \frac{1}{4\pi} \int d\Omega \sum_{l} v_{ps}(|\mathbf{r} - \mathbf{R}_l|) \tag{37}$$

where $v_{ps}(r)$ is the local representation of $\hat{v}_{ps}(\mathbf{r})$. Screening the impurity due to the ion cores is more accurately described in this way, resulting in embedding energies depend upon the local hydrogen environment, i.e., the model is site specific, while maintaining the high symmetry of the jellium. The spherical solid model has met with some success for hydrogen heats of solution in simple metals, and has been further

modified to predict the surrounding metal atom relaxations [14,15]. Further, the spherical solid model is being extended to include the effects of d-bands in transition metals [15]. Since, the spherical solid model is dependent on embedding sites of high symmetry, its use is questionable for understanding the energetics of low symmetry sites found along the diffusion path.

4.4 Corrections to ΔE^{hom}

The embedding energy for slowly varying host metal electron densities, on the order of $\Delta n(\mathbf{r})$, is given by [2]

$$\Delta E(\mathbf{R}_H) \approx \Delta E^{hom}(n_0(\mathbf{R}_H)) \tag{38}$$

where $n_0(\mathbf{R}_H)$ is the host electron density at the site of the hydrogen atom, $\mathbf{R}_H$. Equation 38 is analogous to the homogeneous embedding energy of Eq. 4.8; n_0 being replaced by the true host density at the embedding position.

The use of the total host electron density, in Eq. 38, is somewhat ambiguous since the homogeneous embedding energy, ΔE^{hom}, is based on the valence electron density rather than the total electron density. At metal surfaces and large interstitial sites or vacancies, this is not a severe problem since core electrons are largely localized and contribute only minimally to the total electron density. In transition metals, however, Eq. 38 does not reproduce the trends in the hydrogen heats of solution across the transition metal series [16] indicating that atom-host interactions are important to describing hydrogen in transition metals.

Various models have been proposed which include the impurity-host ion interactions. Generally, the embedding energy in these models is given by

$$\Delta E(\mathbf{R}_H) = \Delta E^{hom}(\overline{n}_0(\mathbf{R}_H)) + \Delta E^{(1)}(\Delta n(\mathbf{R}_H), \mathbf{R}_H) \tag{39}$$

where $\overline{n}_0$ is some suitably average host density at the embedding site, $\mathbf{R}_H$, and $\Delta E^{(1)}$ describes the interaction between the displaced electron density and the potential resulting from the core electrons. Various models have been suggested for the form of $\Delta E^{(1)}$ and for the host density sampling scheme. The most prominent of these are described below.

4.4.1 First Order Perturbation Theory

In the approach of Popovic and Stott [12] and Popovic *et al.* [18], the impurity atom is embedded in the same homogeneous electron gas considered above (thus, $\overline{n}_0 = n_0$) and the impurity-host ion interactions are taken into account through first order perturbation theory. To first order in the bare ion pseudopotential [17], the correction to ΔE^{hom} is given by

$$\Delta E^{(1)}(\mathbf{R}_H) = \sum_l \frac{Z_v Z_H}{|\mathbf{R}_H - \mathbf{R}_l|} + \sum_l \int d\mathbf{r} \Delta\rho(|\mathbf{r} - \mathbf{R}_H|) v_{ps}(|\mathbf{r} - \mathbf{R}_l|) \qquad (40)$$

where $Z_H = 1$ for hydrogen. The first term describes the proton-host interaction and the second term describes the interaction between the ions and the electron cloud that screens the proton. Various studies [16,19,20,21,22,23] using this approach have been implemented for hydrogen in both simple and transition metals. This approach has recently been extended to include the impurity-induced host ion-ion interactions [24].

The self consistency of the displaced electron density for hydrogen in a homogeneous electron gas has been calculated and parameterized by Estreicher and Meier in the density range 2 a.u.$\leq r_s \leq$ 6 a.u. [25]. Subsequent calculations, using local pseudopotentials *via* first order perturbation theory, have been performed to determine potential energy profiles for hydrogen in both simple and transition metals [22]. In most cases the potential energy profiles where strongly dependent on the particular choice of the pseudopotential, $\hat{v}_ps(r)$. Although in some cases the diffusion path could

be inferred (ignoring lattice relaxation) the activation energies and the minimum energy site where semi qualitative or worse. As pointed out by Estreitcher and Meier [25], the local description of the electron-core interaction is probably too crude of an approximation.

4.4.2 Effective medium theory

In the effective medium theory of Stott and Zarremba [2] and Nørskov and Lang [5], the first order correction to ΔE^{hom} is given by:

$$\Delta E^{(1)}(\mathbf{R}_H) = \int d\mathbf{r} \Delta\rho(\mathbf{r} - \mathbf{R}_H)\delta v_{ext}(\mathbf{r}) \tag{41}$$

where $\Delta\rho(\mathbf{r})$ is the total atom induced charge density ($\Delta\rho(\mathbf{r}) = \Delta n(\mathbf{r}) - Z_H\delta(\mathbf{r})$ where Z_H the nuclear charge of the hydrogen atom), and $\delta v_{ext}(\mathbf{r})$ is the difference between the external potentials of the real host and the effective medium. Since $\Delta\rho$ depends upon the density at the embedding site, one must determine the value of n_0 to be used. In practice the value of n_0, chosen is obtained by averaging over the host electron density with a suitably chosen function which samples the local host environment which the impurity interacts. The most common choice is the impurity electrostatic potential where the averaged host density at the embedding site is given as [2,5]

$$\overline{n}_0(\mathbf{R}_H) = \frac{\int \Delta\phi(|\mathbf{r} - \mathbf{R}_H|) n_0(\mathbf{r}) d\mathbf{r}}{\int \Delta\phi(\mathbf{r}) d\mathbf{r}} \tag{42}$$

where $n_0(\mathbf{r})$ is the host electron density and $\Delta\phi(\mathbf{r})$, is the atom induced electrostatic potential given by

$$\Delta\phi(\mathbf{r}) = \int \frac{\Delta\rho(\mathbf{r}')}{|\mathbf{r} - \mathbf{r}'|} d\mathbf{r}' \tag{43}$$

Using the sampled host density, Eq. 42, the first order correction term of Eq. 44, is given by

$$\Delta E^{(1)}(\mathbf{R}_H) = \int \Delta\rho(|\mathbf{r} - \mathbf{R}_H|)\phi_0(\mathbf{r})d\mathbf{r} \tag{44}$$

where the host electrostatic potential, $\phi_0(\mathbf{r})$, is defined as

$$\phi_0(\mathbf{r}) = \int \frac{\rho_0(\mathbf{r}')}{|\mathbf{r} - \mathbf{r}'|}d\mathbf{r}' \tag{45}$$

where $\rho_0(\mathbf{r})$ is the total charge density of the host lattice, i.e.,

$$\rho_0(\mathbf{r}) = n_0(\mathbf{r}) - \sum_l Z_{v_l}\delta(\mathbf{r} - R_l). \tag{46}$$

With $\Delta\phi$ depending upon the sampling density, $\overline{n}_0$, Eq. 42 must be solved self consistently. In cases where $\Delta\phi$ is appreciable compared to the host density, $\overline{n}_0$ is rather insensitive to second order terms, thus self consistency becomes important only when $\Delta\phi \approx 0$. Equation 44 assumes that, while the host electrostatic potential, ϕ_0, may change rapidly away from the impurity atom, the variations are small near the embedding site due to the effective screening in $\Delta\rho$ [26]. The difficulty in this lies in the Friedel oscillations in the displaced hydrogen density, Figure 7. While these oscillations represent only a small contribution to $\Delta\rho$, they interact with the host electrostatic potential near the core regions. The oscillations are largely due to charge conservation; their predicted interaction with the host core potentials tend to give inflated results. In order to take this into account, Nørskov [26] has separated the medium into two parts: a region surrounding the impurity atom and a region further out. Surrounding the impurity, the host potential is slowly varying, and is treated in perturbation theory. Interactions with the Friedel oscillation and the core potential

is taken to infinite order. The resulting embedding energy is given as [7]

$$\Delta E(\mathbf{R}) = \Delta E^{hom}(\overline{n}_0(\mathbf{R})) + \Delta E_c(\mathbf{R}) + \Delta E_v(\mathbf{R}) + \Delta E^{hyb}(\mathbf{R}) \tag{47}$$

where the first term is the homogeneous embedding energy previously discussed, ΔE_c is the first order correction due to the interaction of the impurity atom with the metal atom cores, ΔE_v takes into account the first order shifts in the one electron potential of the host valence electrons due to the impurity and the last term takes into account the hybridization effects between the impurity states and the valence states of the host metal. By restricting the interactions of $\Delta\rho$ to the region surrounding the impurity atom, the sampled electron density of Eq. 42 is given as:

$$\overline{n}_0(\mathbf{R}_H) = \frac{\int_a \Delta\phi_a(|\mathbf{r} - \mathbf{R}_H|) n_0(\mathbf{r}) d\mathbf{r}}{\int_a \Delta\phi_a(\mathbf{r}) d\mathbf{r}} \tag{48}$$

the subscript a indicating that only the region surrounding the impurity atom is to be included, and this region is taken as a sphere of radius R_a. To account for the missing charge in Eq. 48 due to the Friedel oscillations, $\Delta\rho$ is renormalized by adding to Δn the missing charge homogeneously thought the sphere. This has the consequence that the renormalized atom induced potential $\Delta\phi$ is zero outside the sphere. Since the displaced density of the impurity atom interacts with the host over the region where $\Delta\rho$ is appreciable, ΔE_c is given by Eq. 44 with the modification that the integral is only taken over the sphere of radius R_a and $\Delta\rho$ is replaced by the renormalized charged density.

Nørskov [26] found that ΔE_c and ΔE_v roughly scale with the sampled host electron density $\overline{n}_0$ such that

$$\Delta E_c + \Delta E_v \approx -(\alpha_{at} + \alpha_v)\overline{n}_0 = -\alpha_{tot}\overline{n}_0 \tag{49}$$

where α_{tot} was approximately insensitive to the choice of R_a. The corresponding values of of R_a and α_{tot} are [26] 2.5 a_0 and 119 eV/a_0^3 respectively. These two terms were therefore combined with ΔE^{hom} to give an effective homogeneous embedding energy for H in an electron gas where

$$\Delta E_{eff}^{hom} = \Delta E^{hom}(\overline{n}_0) - \alpha_{tot}\overline{n}_0 \tag{50}$$

and is shown in Figure 9 where the parameterized form was given by [26] as

$$\Delta E_{eff}^{hom} = \begin{cases} 130\overline{n}_0 \ln(\overline{n}_0/0.004) - 252\overline{n}_0 - 1.12\ (eV), & 0.002 \leq \overline{n}_0 \leq 0.0127 \\ \\ 398(\overline{n}_0 - 0.0127)^2 + 31\overline{n}_0 - 2.81\ (eV), & 0.0127 \leq \overline{n}_0 \end{cases} \tag{51}$$

the corresponding minimum being at an electron density of $0.0026a_0^{-3}$. Thus, when hydrogen is absorbed into a transition metal it attempts to minimize its interactions by finding a site with low electron density.

4.5 Summary

The theoretical formalism presented in this chapter is the basis for the calculations to be presented in the following chapter. The present theory rests upon the observation that the potential felt by a hydrogen atom from the host lattice appears moslty as a slowly varying function of the electron density along the diffusion path. Further, it is assumed that interactions with the core electrons may be taken into account using perturbation theory as are hybridization effects in the host one electron potential. Since the present model is rooted in the formalism of density functional theory, the inherent limitations of the more empirical potentials discussed in Chapter 2 are largely bypassed. This is to say that we can predict behaviors without resorting to a vast category of experimental electron potential and density data.

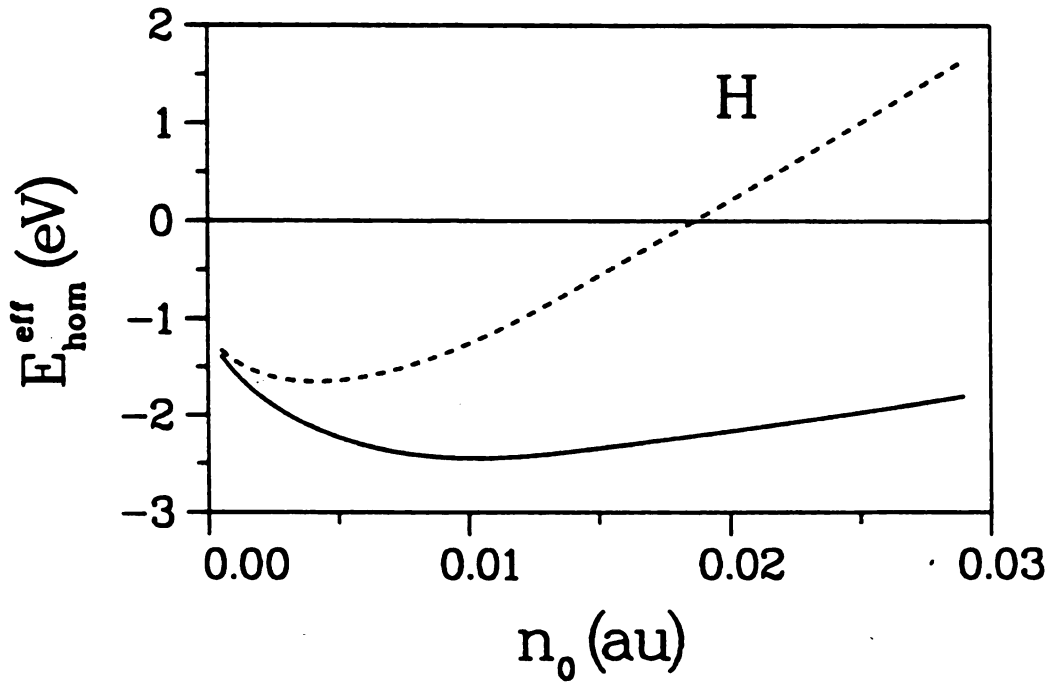

Figure 9: Effective homogeneous embedding energy of hydrogen in a homogeneous electron gas. The homogeneous term E_{hom} is shown by the dashed line for reference.

LIST OF REFERENCES

[1] J. K. Nørskov, Phys. Rev. B **20**, 446 (1979).

[2] M. J. Stott and E. Zaremba, Phys. Rev. B **22**, 1564 (1980).

[3] M. J. Puska, R. M. Nieminen, and M. Manninen, Phys Rev. B **24**, 3037 (1981).

[4] P. Jena and K. S. Singwi, Phys. Rev. B **17**, 3518 (1978).

[5] E. Zaremba, L. M. Sander, H .B. Shores, and J. H. Rose, J. Phys. F **7**, 1763 (1977).

[6] P. Hoenberg and W. Kohn, Phys. Rev. **136**, B864 (1964); W. Kohn and L. J. Sham, Phys. Rev **140**, A1134 (1965).

[7] *Theory of the Inhomogeneous Electron Gas*, Ed. S. Lundqvist and N. H. March (Plenum Press, New York, 1983).

[8] D. M. Ceperley and B. J. Alder, Phys. Rev. Lett. **45**, 566 (1980).

[9] S. H. Vosko, L. Wilk and M. Nusair, Can. J. Phys. 58, 1200 (1980); L. Wilk and S. H. Vosko, J. Phys. C **15**, 2139 (1982).

[10] W. E. Pickett, Comp. Phys. Rep. **9**, 115 (1989).

[11] K. W. Jacobsen, J. K. Nørskov, M. J. Puska, Phys. Rev. B **35**, 7423 (1987).

[12] M. J. Stott and E. Zaremba, Can. J. Phys. **60**, 1145 (1982).

[13] M. Manninen and R. M. Nieminen, J. Phys. F **9**, 1333 (1979); and references therein.

[14] L. M. Kahn, F. Perrot, M. Rasolt, Phys. Rev. B **21**, 5594 (1980).

[15] F. Perrot and M. Rasolt, Phys. Rev. B **23**, 6534 (1981); B **25**, 7327 (1982); B **25**, 7331 (1982)

[16] N. A. Johnston and C. A. Sholl, J. Less-Common Metals **103**, 211(1984).

[17] Z. D. Popovic and M. J. Stott, Phys. Rev. Lett. **33**, 1164 (1974).

[18] Z. D. Popovic, M. J. Stott, J. P. Carbotte and G. R. Piercy, Phys. Rev. B **13**, 590 (1976).

[19] D. S. Larsen and J. K. Nørskov, J. Phys. F **9**, 1975 (1979).

[20] G. Solt, M. Manninen and H. Beck, Solid State Comm. **46**, 295 (1983).

[21] G. Solt, M. Manninen and H. Beck, J. Phys. F **13**, 1379 (1983).

[22] S. Estreicher and P. F. Meier, Phys. Rev. B **27**, 642 (1983).

[23] M. Kaneko, K. Tsuchiya, K. Ohashi, Y. H. Ohashi and M. Fucuchi, J. Phys. F **14**, 1095 (1984).

[24] G. Solt and H. Beck, J. Phys. F **15**, 2085 (1985).

[25] S. Estreicher and P. F. Meier in *Electronic Structure and Properties of Hydrogen in Metals*, Edited by P. Jena and C. B. Satterthwaite (Plenum Press, New York, 1983), pp. 299.

[26] J. K. Nørskov, Phys. Rev. B **26**, 2875 (1982).

[27] P. Nordlander, S. Holloway and J. K. Nørskov, Surface Sci. **136**, 59 (1984).

CHAPTER 5

COMPUTATIONAL METHODOLOGY

5.1 Introduction

The following chapter discusses the computational procedure used in generating the hydrogen potential energy surface in YH_2. The present study assumes that hydrogen-hydrogen interactions are negligible, i.e., the potential energy surface for H in the YH_2 lattice is approximated by that in the pure fcc host lattice, YH_0. The host electron density which plays a fundamental role in the theory is discussed in Section 5.2 and is followed by the hydrogen induced charge density in Section 5.3 and sampling procedure in Section 5.4. In the final section, results for the hydrogen potential energy surface is presented along with a discussion.

5.2 Host Electron Density

As discussed in Chapter 4, the effective medium treats the impurity-metal system as a perturbation of the pure metal host. Thus, in principle the electron density of the pure metal host is required as input into the effective medium theory. Of course in order to obtain the host electron density from *first-principles* calculations would require the solution to Schrödingers wave equation and is equivalent to solving the full problem, i.e., metal plus impurity atom. Obviously, if this was a simple task there would be no need for more approximate methods as the effective medium. However, the computational cost and complexity involved in these *ab initio* calculations is

prohibitive, rather more efficient and less costly schemes are desired which are able to account for most of the observed properties in condensed mater materials. One can however show that approximate solution may be obtained before self consistency is reached. This approximate solution is obtained because the total energy is second order in the electron density [3]. In the case of silicon, reasonable agreement for the charge density have been obtained with only one iteration of the self consistency cycle compared with full self-consistent calculations [3]. However in the case of transition metals and ionic solids, a significant number of iterations are needed to accurately describe the oscillation resulting from charge transfer between ions [4]. An approach such as this would greatly reduces the cost and effort needed in the self consistent solution, while allowing the valence electrons to redistribute themselves thus achieving the minimum in energy *via* the variational principle. This methodology, however, is beyond the scope of the present work, where less costly, more approximate schemes are used. Specifically, the true electron density of the host metal is approximated by a simple linear superposition of radially averaged atomic densities

$$n_0(\mathbf{r}) = \sum_l n_0^{at}(|\mathbf{r} - \mathbf{R}_l|) \tag{52}$$

where the sum extends over the metal lattice vectors $\mathbf{R}_l$, and $n_0^{at}(r)$ is the radially average atomic electron density in a configuration which approximates that found in the pure metal. It should be realized however, that in going from the atomic to solid picture n and l are no longer good quantum numbers. Thus choosing the atomic state used in Eq. 52 is somewhat arbitrary. For most $3d$ transition metals, it has been found that the $3d^n4s^1$ provides a reasonable representation of the true host charge density [5] considering that the total energy is second order in the density [3]. The radially average atomic densities where calculated from the parameterized Hartree-Fock calculations of Clementi and Roetti [1] using a Slater type orbitals (STO) with an extended zeta basis set. The radially averaged electron density in this basis set is

given by:

$$n_0^{at}(r) = \frac{1}{4\pi} \sum_{n,l} N_{nl} \left| \sum_{i_{nl}} R_{i_{nl}}(r) \right|^2 \tag{53}$$

where N_{nl} is the number of electrons in the n^{th} shell of angular momentum l, and the radial functions $R_{i_{nl}}(r)$ are given by

$$R_{i_{nl}}(r) = \sum_{i_{nl}} c_i \frac{(2\zeta_{i_{nl}})^{n_{i_{nl}}+\frac{1}{2}}}{\sqrt{(2n_{i_{nl}})!}} r^{n_{i_{nl}}} \exp(-\zeta_{i_{nl}} r). \tag{54}$$

In what follows the n, l dependence of i will be implied. Both the ground state [Kr]$5s^2 4d^1$, and the excited state, [Kr]$5s^1 4d^2$, have been investigated in the present study. The coefficients for the atomic wave functions, described by Eq. 53 and 54 are given in Table 5. The radial atomic charge density of these two wave functions are graphically shown in Figure 10 where the excited state produces a more compact wave function with the maximum density being pushed inwards by about one atomic unit. The convergence of Eq. 53 is achieved rather rapidly where only nearest and next-nearest neighbors need be considered. Figure 11 displays the convergence for the more diffuse ground state configuration. For both the tetrahedral and octahedral sites, convergence is obtained in approximately $1.2a$ where a is the lattice constant of YH_2 ($a = 9.834$ a.u.) As mentioned in Chapter 2, a is relatively insensitive to both temperature and hydrogen concentration for the fcc dihydride phase and is thus taken as a constant. The simple *ansatz* of Eq. 52 predicts electron densities at interstitial sites of close packed metals, i.e., fcc, bcc, hcp, which are within 10% of self consistent calculations [5]. Due to charge build up between metal atoms due to hybridization of s- and d-orbitals, Eq. 52 will underestimate $n_0(\mathbf{r})$, resulting in a H potential which is probably too soft near the metal atom cores [5]. Thus, away from the metal cores, the approximation is assumed to be a viable representation of the metal electron density.

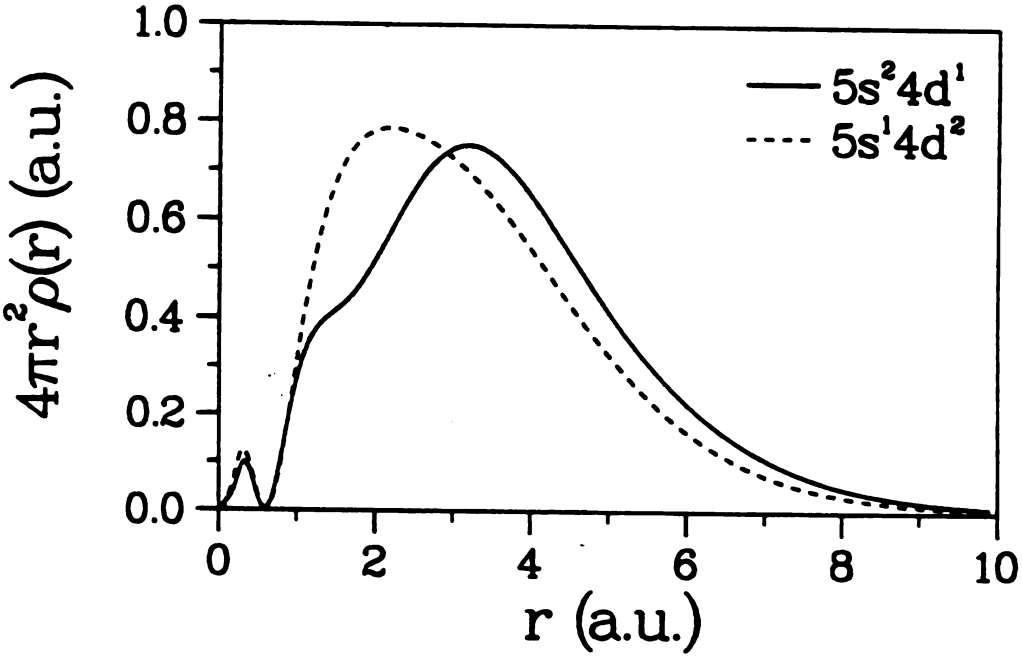

Figure 10: Radial atomic charge densities for the yttrium ground state ($5s^24d^1$) and excited state ($5s^14d^2$) obtained from the Hartree-Fock calculations of Clementi and Roetti [1]

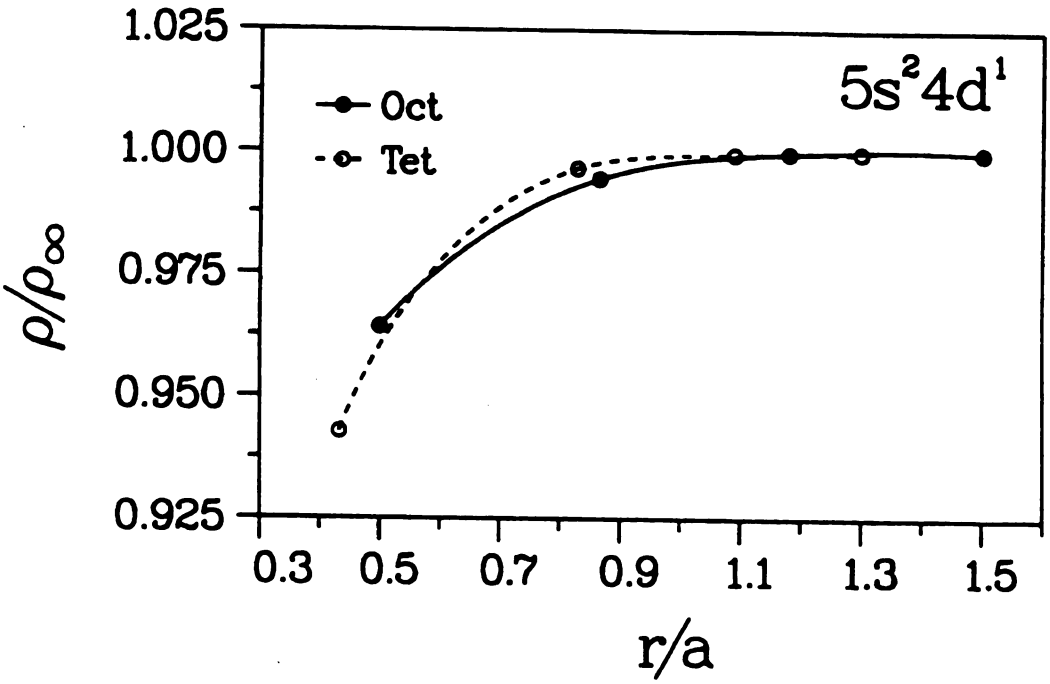

Figure 11: Convergence curves for total valence electron density at tetrahedral and octahedral sites using the atomic yttrium ground state configuration $5s^2 4d^1$

Table 5: Expansion coefficients and exponents for STO basis set for atomic yttrium in the ground and excited state as taken from the Hartree-Fock calculations of Clementi and Roetti [1]

	$[Kr]5s^24d^1$		$[Kr]5s^14d^2$	
nl	ζ_i	c_i	ζ_i	c_i
	$5s^2$		$5s^1$	
1s	40.08530	0.00053	40.08530	0.00056
1s	27.58290	0.02021	27.58290	0.01912
2s	18.66340	0.03676	18.66340	0.03566
2s	16.13290	-0.10770	16.13290	-0.10323
3s	10.36790	0.02124	10.36790	0.02099
3s	7.50901	0.13811	7.50901	0.13017
4s	4.28620	-0.22997	4.28620	0.13017
4s	2.93376	-0.09756	2.93376	-0.09701
5s	1.80195	0.45781	1.84017	0.35987
5s	1.12467	0.54223	1.19254	0.53005
5s	0.80163	0.13061	0.85045	0.23643
	$4d^1$		$4d^2$	
3d	12.92070	-0.05149	12.92070	-0.04579
3d	7.04305	-0.16246	7.04305	-0.14380
4d	4.66942	0.07689	4.68556	0.06558
4d	2.55392	0.55325	2.53176	0.50656
4d	1.29851	0.53220	1.18894	0.60960

5.3 Impurity Induced Electron Density

In order to satisfy the the three conditions placed upon the displaced electron density, i.e., charge conservation:

$$\int d\mathbf{r}\Delta n(\mathbf{r}) = 1 \tag{55}$$

asymptotic behavior:

$$\Delta n\ (r \to \infty) = A\frac{\cos\ (2k_F r + \phi)}{r^3} \tag{56}$$

where A is a constant, ϕ is the phase and k_F is the Fermi wave number where $k_F = (3\pi^2 n_0)^{1/3}$. The last condition is related to the derivative at zero or the cusp condition:

$$\frac{d}{dr}\Delta n(r)\bigg|_{r=0} = -2\Delta n\ (0) \tag{57}$$

where $\Delta n(0)$ is the contact density. Estreicher and Meier [2] have parameterized the displaced electron density $\Delta n(r)$ with the following functional form:

$$\Delta n(r) = \frac{1}{\pi}e^{-2r} + \left(\Delta n\ (0) - \frac{1}{\pi}\right)e^{-2r(1+r)} + f(2k_F r) \tag{58}$$

such that the above three conditions are obtained. The functional form of f, which takes into account of the Friedel oscillations and charge conservation, has been taken as a linear combination of Riccati-Bessel functions which can be expressed in terms of the usual spherical Bessel functions where for the l^{th} order $\hat{j}_l(x) = x j_l(x)$ and is given by

Table 6: Amplitudes of the parametric form for the perturbed charge density as a function of the electron spacing parameter, r_s, as taken from Estreicher and Meier [2].

l	a_l	b_l	c_l	d_l	e_l
$r < Z_2 : A_l = e_l/r_s^4 + d_l r_s^3 + c_l/r_s^2 + b_l/r_s + a_l$					
0	-0.018	0.696	-4.422	10.795	-9.879
1	-0.103	0.927	-1.711	2.257	0.347
2	0.233	-2.769	10.200	-20.780	14.900
3	-0.156	1.946	-8.380	17.681	-15.040
$r > Z_2 : B_l = e_l/r_s^4 + d_l r_s^3 + c_l/r_s^2 + b_l/r_s + a_l$					
2	0.047	-0.379	-1.256	5.882	-6.197
3	-0.120	1.631	-6.186	6.326	-4.056
4	0.122	-1.688	6.083	-6.313	2.388
5	-0.114	1.820	-9.391	19.463	-16.430

$$
\begin{aligned}
f(x) &= \frac{A_0}{x^4+1}\hat{j}_0(x)(1-e^{-x}) + \frac{1}{x^3+1}\sum_{l=1}^{3} A_l\,\hat{j}_l(x)\;;\; r < Z_2 \\
&= \frac{1}{x^3+1}\sum_{l=2}^{5} B_l\,\hat{j}_l(x)\;;\; r > Z_2
\end{aligned}
\tag{59}
$$

where Z_2 is the second root of the displaced charge density and is linear in r_s where $Z_2 = 1.52r_s + 0.462$. The contact density was chosen such that at large values of r_s, $\Delta n(0)$ approached the free hydrogen atom solution; the functional form being given by [2]:

$$
\Delta n(0) = \frac{1}{\pi} + \exp(-0.72 - 1.28\ln r_s - 0.384\ln^2 r_s) \tag{60}
$$

The coefficients of the parameterization of f is given in Table 6.

5.4 Sampled Host Electron Density

Due to the large lattice spacing in YH_2, the interstitial electron density of the pure metal lattice occurs near the minimum of ΔE_{eff}^{hom}. Care must therefore be taken when calculating the averaged host electron density as given by Eq. 13, since small perturbations of $\overline{n}_0$ may drastically change the PES around the minimum; and more importantly the relative energy between various sites. With the overlapping *ansatz* of Eq. 17, the sampled electron density is given by

$$\overline{n}_0(\mathbf{R}_H) = \sum_{\mathbf{R}_l} -\frac{1}{\alpha_{at}} \int_a \Delta\phi_a(r)\, n_0^{at}(|\mathbf{r} - \mathbf{R}_l + \mathbf{R}_H|) d\mathbf{r}\,; \tag{61}$$

where the origin of integration is centered on the hydrogen atom and

$$\alpha_{at} = -\int_a \Delta\phi_a(\mathbf{r}) d\mathbf{r}. \tag{62}$$

Rather than using a three dimensional numerical quadrature scheme on the sampled electron density, which subsequently has to be calculated at each point along the diffusion path, the sampled electron density may be rewritten as

$$\overline{n}_0(\mathbf{R}_H) = \sum_{\mathbf{R}_l} \overline{n}_0{}^{at}(|\mathbf{R}_H - \mathbf{R}_l|) \tag{63}$$

where the normalized atomic contribution to the sampled electron density is given by

$$\overline{n}_0{}^{at}(|\mathbf{R}_H - \mathbf{R}_l|) = -\frac{1}{\alpha_{at}} \int_a \Delta\phi_a(r) n_0^{at}(|\mathbf{r} - \mathbf{R}_l + \mathbf{R}_H|) d\mathbf{r}. \tag{64}$$

The atomic density, being radially averaged, is nothing more than a linear combination of STO's centered at $\mathbf{R}_l - \mathbf{R}_H$. The integrand in Eq. 64 is a product of two radially symmetric functions about different centers, depending only upon the radial

distance between the hydrogen atom and a given lattice vector. The two center integral is simplified by using the method proposed by Harris [6] where the STO's are translated to the origin of integration. In this method, the radial dependence may be expressed as

$$R^{n-1}\exp(-\zeta R) = \zeta^{n-1}\sum_{k=0}^{\infty} V^0_{n,0,k}(\zeta r, \zeta R)\mathrm{P}_k(\cos\theta) \tag{65}$$

where R is the local radial coordinate of the center $\mathbf{R}_l - \mathbf{R}_H$, P_k is the k^{th} Legendre polynomial and the function $V^0_{n,0,k}$ is defined as

$$V^0_{n,0,k}(\zeta r, \zeta R) = \zeta^{n-1}\frac{2k+1}{2rR}\int_{|R-r|}^{R+r} r_a^n \exp(-\zeta r_a)d\mathbf{r}_a. \tag{66}$$

Using Eq. 53 and 54, the atomic density is given by

$$n_0^{at}(r) = \sum_{nl} N_{nl}\sum_{i,j} c_i' c_j' r^{n_{ij}-2}\exp(-\zeta_{ij}r)/4\pi \tag{67}$$

where $c_i' = c_i[(2n_i)!]^{-\frac{1}{2}}(2\zeta_i)^{n_i+\frac{1}{2}}$ with $n_{ij} = n_i + n_j$ and $\zeta_{ij} = \zeta_i + \zeta_j$ such that the electron density may be put into the form of Eq 65. Translating Eq. 67 to the origin of integration *via* Eq. 65 and 66 and using the orthogonality property of Legendre polynomials one may rewrite the sampled host electron density in the form:

$$\overline{n}_0{}^{at}(R) = \frac{-1}{2R\alpha_{at}}\sum_{nl} N_{nl}\sum_{i,j}\sum_{k=0}^{n_{ij}-1}\zeta_{i,j}^{-(k+1)}\frac{(n_{ij}-1)!}{(n_{ij}-k-1)!}I_a(R; R_a, n_{ij}, \zeta_{ij}) \tag{68}$$

where $I_a(n, \zeta; R, r)$ is given by

$$I_a(R; R_a, n, \zeta) = \int_0^{R_a}\Big(|R-r|^{n-k-1}e^{-\zeta|R-r|} - (R+r)^{n-k-1}e^{-\zeta(R+r)}\Big)\Delta\phi_a(r)rd\mathbf{r} \tag{69}$$

Although the above equation looks rather formidable, it is much simpler to evaluate using high order integration methods than the three dimensional integral, Eq. 61. In

cases were the impurity induced electrostatic potential is small and $\overline{n}_0$ must be solved self-consistently, a large savings in computational time is gained. Further, one may evaluate Eq. 68 for a range of distances: $R_a \leq R \leq R_{max}$ were R_{max} is the longest vector to be considered in the summation. One can use this information in a look up table or use a parameterized from resulting in evaluations which are as easy as calculating the host electron density. In the actual calculations the absolute value signs of Eq. 69 may be dropped as the hydrogen sphere is constrained not to overlap with the metal atom cores, i.e., $R \leq R_a$. Using the above methodology to evaluate $\overline{n}_0$ and the parameterized form of ΔE_{eff}^{hom} in Eq. 51 one may evaluate the potential energy for hydrogen diffusion through a transition metal lattice with as much ease as a two body potential.

5.5 Results

In Figures 12 and 13 the results for sampled host electron density predicted by Eq. 68 for the atomic ground state and excited states are shown as well as the host electron density corresponding to the overlapping *ansatz* of Eq. 52. The hydrogen diffusion path in these figures corresponds to motion along the [111] direction of the fcc lattice where the parameter t describes this high symmetry path. The tetrahedral sites are located at $t = 0.25$ and 0.75 whereas the octahedral site is located at 0.5. In both cases, the electron density at the octahedral site leads to a much lower density than the tetrahedral site. This is easily seen by considering the maximum volume a hydrogen may occupy in the the touching sphere formalism where the octahedral site occupies ~ 6 times more volume than a tetrahedral site [2]. From this observation alone one would expect that the octahedral site would be the more stable site. In fact, for most fcc metals this is usually the case since the electron density at the octahedral site is lower thereby resulting in a more stable site as can be inferred from Figure 9. However, in the case of the yttrium dihydride system, the large

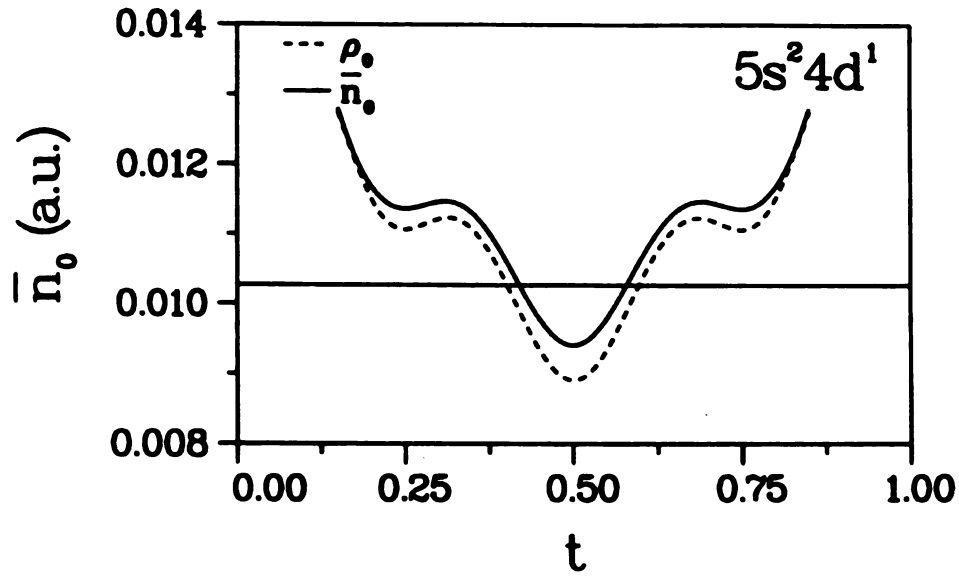

Figure 12: Sampled host electron density for the hydrogen T-O-T diffusion path with the atomic wavefunctions taken from the ground state configuration, $5s^24d^1$. The host density is shown by the dashed curve.

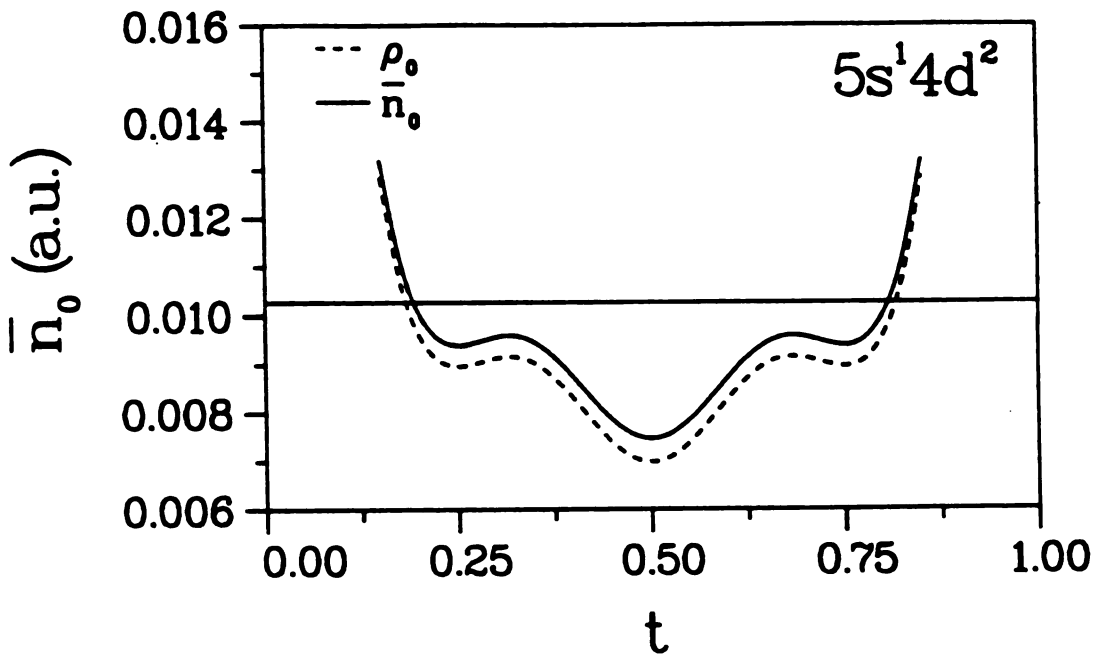

Figure 13: Sampled host electron density for the hydrogen T-O-T diffusion path with the atomic wavefunctions taken from the excited state configuration, $5s^14d^2$. The host density is shown by the dashed curve.

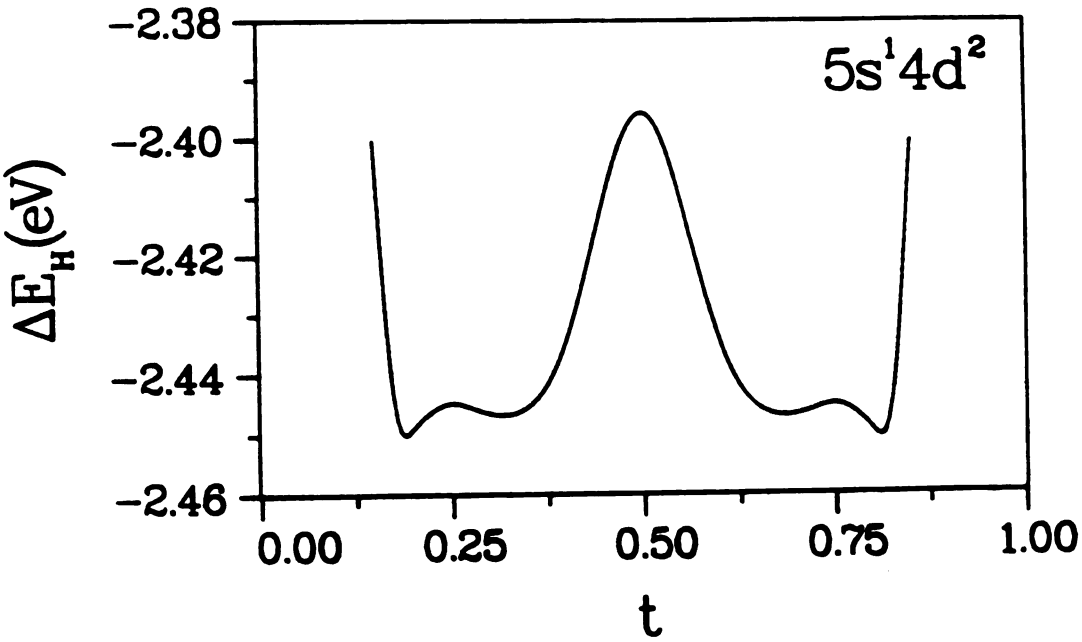

Figure 14: Hydrogen potential energy surface for the T-O-T diffusion path as predicted by the effective medium theory with the atomic wavefunctions taken from the ground state configuration ($5s^14d^2$)

lattice constant results in and unusually small electron densities as predicted from the overlapping atomic density approximation. Thus the density may be smaller than the minimum of ΔE_{eff}^{hom} leading to the observation that a decrease in density leads to higher energies. This is exactly the case in the present study. The electron density giving the minimum in ΔE_{eff}^{hom} is shown by the solid line in Figures 12 and 13. In the case of the excited state wave function, $5s^14d^2$, the sampled electron density is always smaller than this minimum value resulting in a situation were the energy decrease with increasing electron density. The corresponding embedding energy is shown in Figure 14 where neither the tetrahedral or the octahedral site is a minimum. This

is in strong disagreement with experimental results discussed in Chapter 2. Further, with the minimum in ΔE_{eff}^{hom} so close to the values of $\overline{n}_0$ calculated with the excited state wave function, one questions the validity of the overlapping *ansatz* where even a small perturbation in the wave function can result in large changes in the potential energy surface.

The sensitivity to the chosen wave function is clearly seen in Figure 15 where the potential energy surface for the ground state wave function is shown. In this case the n_0^{min} is intermediate between the density corresponding the to tetrahedral and octahedral sites resulting in a potential energy surface with a minima at the tetrahedral site but a maximum at the octahedral site. It is entirely possible that the wave function is delocalized such the the embedding energy at the octahedral site is stable. However, this would require solving Schrödingers wave equation for the present potential and is beyond the scope of the present work. Even if one were to solve Schrödingers wave equation, the results would be questionable due to the sensitivity of the atomic wavefunctions. It should be realized however, that the energies calculated here are in agreement with calculations for hydrogen in the hcp lattice as performed by Nordlander [7]. However, at the present level of sophistication the method is lacking in the ability to model the potential energy surface of hydrogen in the YH_0 lattice. Without detailed calculations concerning the hydrogen-hydrogen interactions, we are not able to discern whether differences are due to the present model or whether hydrogen-hydrogen interactions are important.

5.6 summary

The present chapter has outlined the general formalism for obtaining the sampled host electron density. Specific emphasis was placed upon a new method which is as easy to calculate as the metal electron density in the overlapping *ansatz*. It was found that for both the ground and excited state atomic wave function of yttrium

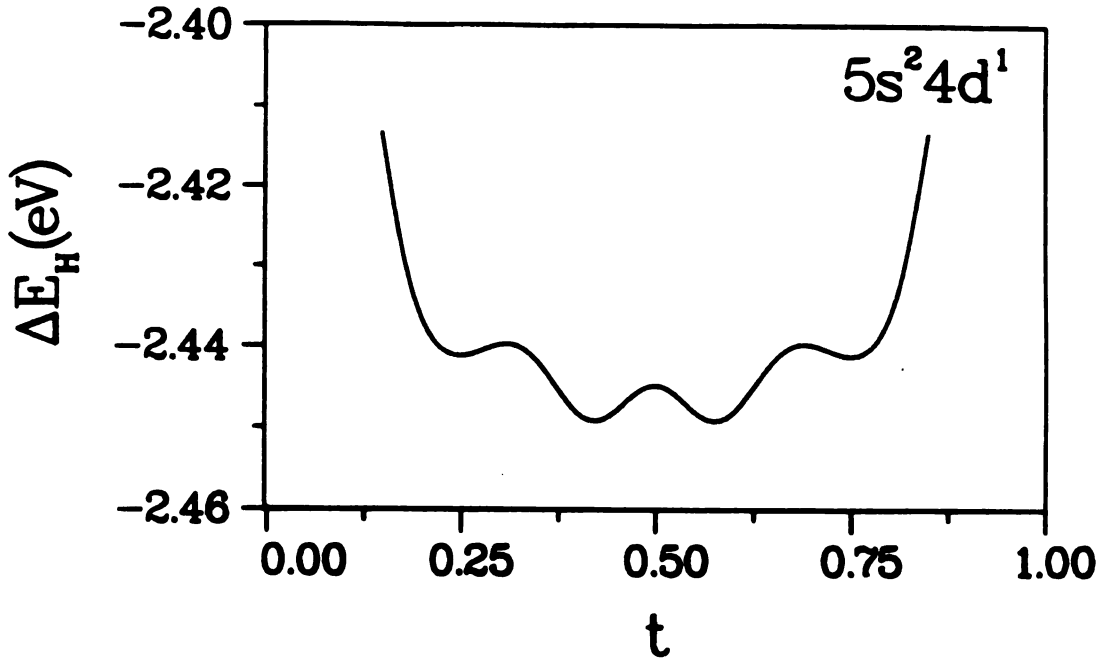

Figure 15: Hydrogen potential energy surface for the T-O-T diffusion path as predicted by the effective medium theory with the atomic wavefunctions taken from the ground state configuration ($5s^2 4d^1$)

gave results which appear to be in disagreement with experimental studies. This discrepancy being attributed to the the host electron density approximation. In the yttrium dihydride system, the lattice constant is such that the choice of the atomic wave function is and extremely sensitive variable in the calculations.

LIST OF REFERENCES

[1] E. Clementi and C. Roetti, *Atomic Data and Nuclear Data Tables* (Academic, New York, 1974), Vol. 14 Nos. 3 and 4.

[2] S. Estreicher and P.F. Meier in *Electronic Structure and Properties of Hydrogen in Metals*, Edited by P.Jena and C.B. Satterthwaite (Plenum Press, New York, 1983), pp. 299; Phys. Rev. B**27**, 642 (1983).

[3] J. R. Chelikowsky and S. G. Louie, Phys. Rev. B**29**, 3470 (1984).

[4] J. R. Chelikowsky, Personal communication.

[5] J. K. Nørskov, Phys. Rev. B **26**, 2875 (1982).

[6] F.E. Harris, J. Chem. Phys. **43**, S165 (1965).

[7] P. Nordlander, J. K. Nørskov and F. Besenbacher, J. Phys. F **16**, 1161 (19886).